



CHORUS

This is the accepted manuscript made available via CHORUS. The article has been published as:

$K \rightarrow \pi\pi$ $\Delta I=3/2$ decay amplitude in the continuum limit

T. Blum, P. A. Boyle, N. H. Christ, J. Frison, N. Garron, T. Janowski, C. Jung, C. Kelly, C. Lehner, A. Lytle, R. D. Mawhinney, C. T. Sachrajda, A. Soni, H. Yin, and D. Zhang ((RBC and UKQCD Collaborations))

Phys. Rev. D **91**, 074502 — Published 6 April 2015

DOI: [10.1103/PhysRevD.91.074502](https://doi.org/10.1103/PhysRevD.91.074502)

$K \rightarrow \pi\pi$ $\Delta I = 3/2$ decay amplitude in the continuum limit.

T.Blum,^{1,2} P.A.Boyle,³ N.H.Christ,⁴ J.Frison,³ N.Garron,^{5,6} T.Janowski,⁷ C.Jung,⁸ C.Kelly,²
 C.Lehner,⁸ A.Lytle,⁹ R.D. Mawhinney,⁴ C.T.Sachrajda,⁷ A.Soni,⁸ H.Yin,⁴ and D.Zhang⁴
 (RBC and UKQCD Collaborations)

¹*Physics Department, University of Connecticut, Storrs, CT 06269-3046, USA*

²*RIKEN-BNL Research Center, Brookhaven National Laboratory, Upton, NY 11973, USA*

³*SUPA, School of Physics, The University of Edinburgh, Edinburgh EH9 3JZ, UK*

⁴*Physics Department, Columbia University, New York, NY 10027, USA*

⁵*DAMTP, University of Cambridge, Wilberforce Road, Cambridge CB3 0WA, UK*

⁶*School of Computing and Mathematics, Plymouth University Plymouth, PL4 8AA, UK*

⁷*School of Physics and Astronomy, University of Southampton, Southampton SO17 1BJ, UK*

⁸*Brookhaven National Laboratory, Upton, NY 11973, USA*

⁹*SUPA, School of Physics and Astronomy, University of Glasgow, Glasgow, G12 8QQ, UK*

We present new results for the amplitude A_2 for a kaon to decay into two pions with isospin $I = 2$: $\text{Re}A_2 = 1.50(4)_{\text{stat}}(14)_{\text{syst}} \times 10^{-8}$ GeV; $\text{Im}A_2 = -6.99(20)_{\text{stat}}(84)_{\text{syst}} \times 10^{-13}$ GeV. These results were obtained from two ensembles generated at physical quark masses (in the isospin limit) with inverse lattice spacings $a^{-1} = 1.728(4)$ GeV and $2.358(7)$ GeV. We are therefore able to perform a continuum extrapolation and hence largely to remove the dominant systematic uncertainty from our earlier results [1, 2], that due to lattice artefacts. The only previous lattice computation of $K \rightarrow \pi\pi$ decays at physical kinematics was performed using an ensemble at a single, rather coarse, value of the lattice spacing ($a^{-1} \simeq 1.37(1)$ GeV). We confirm the observation reported in [3] that there is a significant cancellation between the two dominant contributions to $\text{Re}A_2$ which we suggest is an important ingredient in understanding the $\Delta I = 1/2$ rule, $\text{Re}A_0/\text{Re}A_2 \simeq 22.5$, where the subscript denotes the total isospin of the two-pion final state. Our result for A_2 implies that the electroweak penguin contribution to ϵ'/ϵ is $\text{Re}(\epsilon'/\epsilon)_{\text{EWP}} = -(6.6 \pm 1.0) \times 10^{-4}$.

PACS numbers: 11.15.Ha, 11.30.Rd, 12.15.Ff, 12.38.Gc

I. INTRODUCTION

Nonleptonic $K \rightarrow \pi\pi$ decays continue to be an important class of processes in the phenomenology of the standard model of particle physics. Historically it was in these decays that both direct and indirect CP-violation were discovered and the challenges for theoretical physicists include an explanation of the long-standing puzzle of the $\Delta I = 1/2$ rule and an *ab initio* computation of ϵ'/ϵ . Developments in the theoretical framework of Lattice QCD and in efficient algorithms, together with the availability of the latest computing power, have made meeting these challenges feasible. A significant element of the current joint research program of the RBC and UKQCD collaborations is the evaluation of the $K \rightarrow \pi\pi$ amplitudes A_0 and A_2 , where the subscript represents the isospin of the two-pion final state (which by Bose symmetry is restricted to 0 or 2). In this paper we present our latest results for A_2 .

In [1, 2] we reported on the first results from a lattice determination of the amplitude A_2 for $K \rightarrow (\pi\pi)_{I=2}$ decays, where I is the total isospin of the two-pion final state:

$$\text{Re}A_2 = 1.381(46)_{\text{stat}}(258)_{\text{syst}} 10^{-8} \text{ GeV}, \quad \text{Im}A_2 = -6.54(46)_{\text{stat}}(120)_{\text{syst}} 10^{-13} \text{ GeV}. \quad (1)$$

This was the first quantitative calculation of an amplitude for a realistic hadronic weak decay and hence extended the framework of lattice simulations into the important domain of nonleptonic weak decays. As explained in the Introduction of [2], in order to obtain the result in Eq. (1) it was necessary to overcome a number of theoretical problems and exploit recent improvements in algorithms and the opportunities provided by increases in computing resources. The systematic errors in (1) are dominated by the fact that the calculation was performed at a single, rather coarse, value of the lattice spacing ($a \simeq 0.14$ fm). We estimated these errors to be $O(15\%)$.

In this paper we repeat the calculation at two finer values of the lattice spacing and perform the continuum extrapolation. The simulations are carried out at physical pion masses (with unitary sea and valence quark masses) using our two new ensembles with lattice spacings $a = 0.011$ fm and $a = 0.084$ fm. Our new result is presented in Eq. (63) and we reproduce it here for the reader's convenience:

$$\boxed{\text{Re}(A_2) = 1.50(4)_{\text{stat}}(14)_{\text{syst}} \times 10^{-8} \text{ GeV}; \quad \text{Im}(A_2) = -6.99(20)_{\text{stat}}(84)_{\text{syst}} \times 10^{-13} \text{ GeV}.} \quad (2)$$

A very interesting feature of our earlier calculation of A_2 was the observation that the two dominant contributions

to $\text{Re } A_2$ show a significant numerical cancellation [3]. We argued in [3] that this cancellation is an important element in the explanation of the $\Delta I = 1/2$ rule, $\text{Re } A_0/\text{Re } A_2 \simeq 22.5$. We confirm this cancellation in the present calculation. Of course, before we can claim that we fully understand the $\Delta I=1/2$ rule, we need to compute A_0 at physical quark masses and momenta; this calculation is even more challenging than the evaluation of A_2 but is underway. For the status of this calculation we refer the reader to [4].

The structure of the remainder of this paper is as follows. In the next section we present the parameters of the two ensembles used in this calculation. The evaluation of the bare matrix elements and the renormalization of the lattice operators are discussed in Secs. III and IV respectively. We consider finite-volume effects in Sec. V and present an overview of the different sources of systematic uncertainty in Sec. VI. We perform the continuum extrapolation in Sec. VII and present our final result in Eq. (63). Sec. VIII contains our conclusions and a brief discussion of the prospects for the reduction of the errors in A_2 as well as for the calculation of A_0 . There is one appendix in which we reproduce the calculation from [5] of the Lellouch-Lüscher factor for finite-volume corrections in the context of chiral perturbation theory. This calculation demonstrates how to disentangle the finite volume corrections which decrease exponentially with increasing lattice volume (a source of systematic error) from those which decrease as a power of the volume (which are corrected by the Lellouch-Lüscher factor). This calculation also clarifies a misunderstanding of these effects in the literature [6].

II. DETAILS OF THE SIMULATION

The calculations described below have been performed on two new 2+1 flavor ensembles generated with the Iwasaki gauge action and with Möbius domain wall fermions [7]. The parameters of the ensembles are:

- (i) $48^3 \times 96 \times 24$ with $\beta = 2.13$ ($a^{-1} = 1.728(4)$ GeV);
- (ii) $64^3 \times 128 \times 12$ with $\beta = 2.25$ ($a^{-1} = 2.357(7)$ GeV).

These two ensembles use the Möbius variant of domain wall fermions [8] with a Möbius scale factor $\alpha = 2$. For compactness of notation we will refer to these ensembles as 48^3 and 64^3 respectively. The lattice spacing and quark masses were set by choosing the masses of the pion, kaon and the Ω -baryon to be equal to their physical values. The corresponding sea quark masses are $am_{ud} = 7.8 \times 10^{-4}$ and $am_s = 3.62 \times 10^{-2}$, with the residual mass $am_{res} = 6.19(6) \times 10^{-4}$ for the 48^3 ensemble and $am_{ud} = 6.78 \times 10^{-4}$, $am_s = 2.661 \times 10^{-2}$ and $am_{res} = 2.93(8) \times 10^{-4}$ for the 64^3 ensemble. The two ensembles have approximately the same physical volume with spatial extent $L \simeq 5.5$ fm, enabling the continuum extrapolation to be separated from finite-volume effects which we estimate separately. For more details on these ensembles see [7] and we will return briefly to the determination of the lattice spacings in the context of the continuum extrapolation in Sec. VII.

The results presented below were obtained using 76 gauge configurations on the 48^3 ensemble and 40 on the 64^3 ensemble. The large statistical uncertainty one expects with a relatively small number of gauge configurations can be significantly reduced if we perform many measurements on each configuration in which the sources and sinks are simply translated in space and time [7]. Performing multiple measurements on the same configuration offers two important opportunities for increased efficiency. First if we can use a low-mode deflation method such as eigCG [9] we will be able to amortize the set-up costs of such an approach over a large number of inversions. Second we can use the all mode averaging technique [10] and perform most of these many inversions at reduced precision and use a relatively few accurate inversions to determine a correction that guarantees systematic double precision but with an additional (usually small) statistical error that reflects the small number of accurate solves. Specifically for the 48^3 ensemble, the eigCG method was used in single precision with 600 approximate low-lying eigenvectors and a stopping residual of 10^{-4} . The approximate (wall source) propagators were computed on all 96 time slices. The accurate solves used to correct the approximation were computed on time slices 0, 76, 72, 68, 64, 60 and 56 with CG stopping residual 10^{-8} . (This choice of time-slice separations is not related to the $K \rightarrow \pi\pi$ calculation presented here but to an accompanying calculation of B_K [7].) To ensure that no bias results from the choice of inexact solves for which the correction is calculated, this complete pattern of source time slices for the accurate solves was shifted by a different random time displacement on each configuration. A similar procedure was used on the 64^3 ensemble but with 1500 low-modes and a stopping residual of 10^{-5} for the approximate solves and accurate solves on time slices 0, 103, 98, 93, 88, 83, 78 and 73. On both the ensembles, the accurate CG solves were also computed using eigCG, exploiting the approximate eigenvectors created during the inaccurate applications of eigCG.

Measurements on the 48^3 and 64^3 ensembles are separated by 20 MD and 40 MD units respectively. In order to study the effects of autocorrelations we bin the data. We find that the effects are small, typically leading to a variation of the statistical errors of less than 10%. The results presented below were obtained after binning the 76 configurations of the 48^3 ensemble into 19 bins of 4 configurations and the 40 configurations of the 64^3 ensemble into 8 bins of 5

	m_π	m_K	$E_{\pi\pi}$	$m_K - E_{\pi\pi}$
48^3 (lattice units)	$8.050(13) \times 10^{-2}$	$2.8867(15) \times 10^{-1}$	$2.873(13) \times 10^{-1}$	$1.4(14) \times 10^{-3}$
64^3 (lattice units)	$5.904(14) \times 10^{-2}$	$2.1531(14) \times 10^{-1}$	$2.1512(68) \times 10^{-1}$	$9(10) \times 10^{-4}$
48^3 (MeV)	139.1(2)	498.82(26)	496.5(16)	2.4(24)
64^3 (MeV)	139.2(3)	507.4(4)	507.0(16)	2.1(26)

TABLE I: Pion and kaon masses and the $I=2$ two-pion energies in lattice and physical units measured on the 48^3 and 64^3 ensembles. The momentum of each of the final-state pions is $\pm\pi/L$ in each of the three spatial directions.

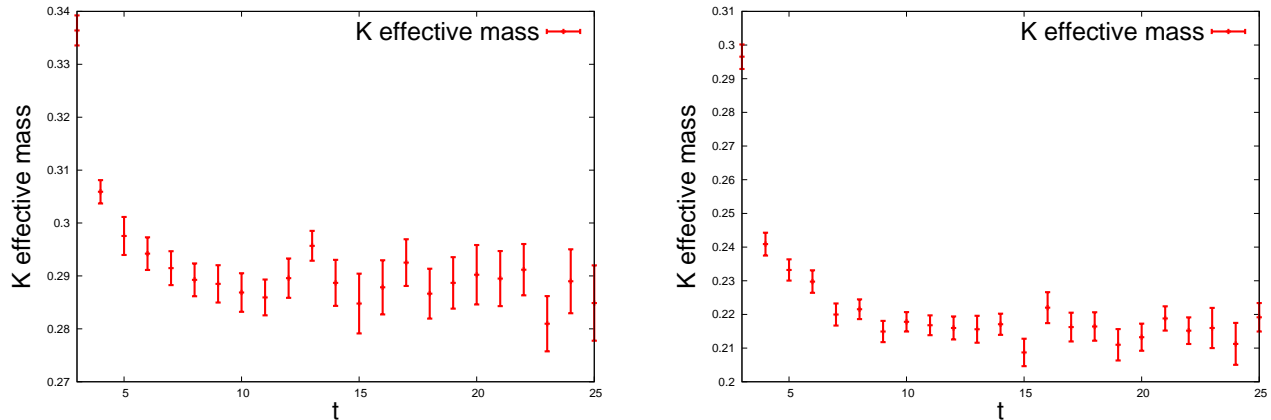


FIG. 1: Effective mass plots for the kaon correlation functions on the 48^3 ensemble (left) and 64^3 ensemble (right).

configurations. The 40 configurations from the 64^3 ensemble are precisely those used in the global analysis reported in [7]. The 76 configurations from the 48^3 ensemble include 73 of the 80 used in [7]. We have however, repeated the relevant analysis of [7], including the determination of the lattice spacings, using precisely the 76 configurations for which we have computed A_2 . This makes it possible to compute standard jackknife errors for our physical results which necessarily depend upon the value of the lattice spacing.

The pion (m_π) and kaon masses (m_K) as well as the energies of the $I = 2$ two-pion state ($E_{\pi\pi}$) obtained on the two ensembles are shown in Tab. I. The fitting ranges used for pion and kaon masses as well as two pion energies were from 10 to 86 on the 48^3 ensemble and from 10 to 118 on the 64^3 ensemble. These choices were motivated by the plateaus in the effective mass plots shown in figures 1-2. The effective mass of the kaon, m_K^{eff} , is defined numerically by the ratio:

$$\frac{C_K(t+1)}{C_K(t)} = \frac{\cosh(m_K^{\text{eff}}(t+1 - T/2))}{\cosh(m_K^{\text{eff}}(t - T/2))}, \quad (3)$$

and the two-pion effective mass, $E_{\pi\pi}^{\text{eff}}$, is found by inverting:

$$\frac{C_{\pi\pi}(t+2) - C_{\pi\pi}(t+1)}{C_{\pi\pi}(t+1) - C_{\pi\pi}(t)} = \frac{e^{-E_{\pi\pi}^{\text{eff}}(t+2)} + e^{-E_{\pi\pi}^{\text{eff}}(T-t-2)} - e^{-E_{\pi\pi}^{\text{eff}}(t+1)} + e^{-E_{\pi\pi}^{\text{eff}}(T-t-1)}}{e^{-E_{\pi\pi}^{\text{eff}}(t+1)} + e^{-E_{\pi\pi}^{\text{eff}}(T-t-1)} - e^{-E_{\pi\pi}^{\text{eff}}t} + e^{-E_{\pi\pi}^{\text{eff}}(T-t)}}. \quad (4)$$

The two-point correlation functions C_K and $C_{\pi\pi}$ are defined explicitly in Eq. (22) below and the differences in the numerator and denominator on the left-hand side of Eq. (4) are introduced to eliminate the constant C in Eq. (23).

The pion and kaon masses correspond closely to their physical values. We will explain below that the pions are given a momentum π/L in each of the three spatial directions and from the table we see that with this choice $E_{\pi\pi} \simeq m_K$ and the $K \rightarrow \pi\pi$ matrix elements correspond to the on-shell (within statistical errors) decay of a kaon in the centre-of-mass frame. We now discuss the evaluation of the matrix elements.

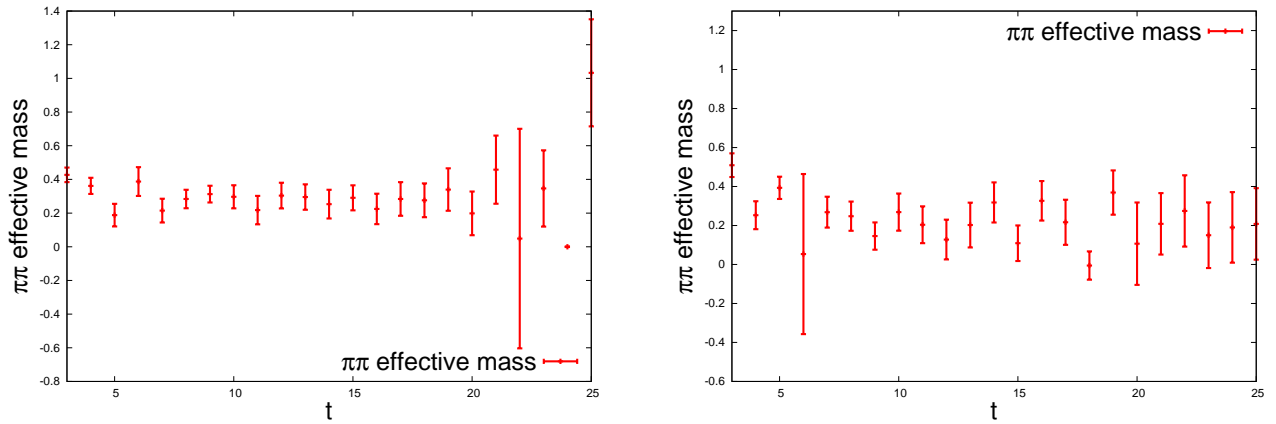


FIG. 2: Effective mass plots for the two-pion correlation functions on the 48^3 ensemble (left) and 64^3 ensemble (right).

III. EVALUATION OF THE BARE MATRIX ELEMENTS

$K \rightarrow \pi\pi$ decay amplitudes are defined by:

$$\sqrt{2} A_{2,0} e^{i\delta_{2,0}} = \langle (\pi\pi)_{I=2,0} | H_W | K^0 \rangle, \quad (5)$$

where H_W is the component of the weak Hamiltonian which changes the strangeness by one unit. The weak Hamiltonian can be separated into short and long distance contributions by using the operator product expansion:

$$H_W = \frac{G_F}{\sqrt{2}} V_{ud}^* V_{us} \sum_i C_i(\mu) Q_i(\mu), \quad (6)$$

where G_F is the Fermi constant, V_{us} and V_{ud} are CKM matrix elements, the Q_i are all the possible dimension-6 operators which contribute to the decay and C_i are the corresponding Wilson coefficients which contain information about the short distance physics. The C_i take the form $C_i = z_i + \tau y_i$ where τ is the ratio of CKM matrix coefficients $\tau = -\frac{V_{ts}^* V_{td}}{V_{us}^* V_{ud}}$.

In this paper we only consider $\Delta I = 3/2$ decays where the two-pion final state has total isospin 2. The nonperturbative contribution to the decay amplitude is contained in the matrix elements:

$$M_i^{K^0} \equiv \langle (\pi\pi)_{I_3=0}^{I=2} | Q_{\Delta I_3=1/2,i}^{\Delta I=3/2} | K^0 \rangle \quad \text{and} \quad M_i^{K^+} \equiv \langle (\pi\pi)_{I_3=1}^{I=2} | Q_{\Delta I_3=1/2,i}^{\Delta I=3/2} | K^+ \rangle. \quad (7)$$

There are only 3 operators which contribute to A_2 , which we label according to their chiral $SU(3)_L \times SU(3)_R$ transformation properties. We have one (27,1) operator and two electroweak penguin operators labelled (8,8) and $(8,8)_{\text{mx}}$, where the subscript mx denotes a color mixed operator. Explicitly, the operators are given by:

$$Q_{(27,1)}^{\Delta I=3/2} = (\bar{s}_i d_i)_L (\bar{u}_j u_j - \bar{d}_j d_j)_L + (\bar{s}_i u_i)_L (\bar{u}_j d_j)_L, \quad (8)$$

$$Q_{(8,8)}^{\Delta I=3/2} = (\bar{s}_i d_i)_L (\bar{u}_j u_j - \bar{d}_j d_j)_R + (\bar{s}_i u_i)_L (\bar{u}_j d_j)_R, \quad (9)$$

$$Q_{(8,8)_{\text{mx}}}^{\Delta I=3/2} = (\bar{s}_i d_j)_L (\bar{u}_j u_i - \bar{d}_j d_i)_R + (\bar{s}_i u_j)_L (\bar{u}_j d_i)_R. \quad (10)$$

The subscripts L and R denote the left and right-handed spin structures respectively:

$$(\bar{q}_1 q_2)_L = \bar{q}_1 \gamma^\mu (1 - \gamma^5) q_2 \quad \text{and} \quad (\bar{q}_1 q_2)_R = \bar{q}_1 \gamma^\mu (1 + \gamma^5) q_2. \quad (11)$$

The Lorentz indices are understood to be contracted between the two parentheses in each of the operators in Eqs. (8)-(10) and i, j are color indices which are summed from 1 to 3.

Below we will confirm the feature found in our earlier work [1, 2] that the dominant contribution to $\text{Re}(A_2)$ comes from (27,1) operator, while the dominant contribution to $\text{Im}(A_2)$ in the $\overline{\text{MS}}$ scheme at 3 GeV comes from the $(8,8)_{\text{mx}}$

operator. We can now write the expressions for the A_2 amplitude, which is:

$$A_2 = \frac{G_F}{\sqrt{2}} V_{ud}^* V_{us} \sum_i C_i(\mu) \left(\frac{1}{\sqrt{2}} M_i^{K^0} \right) = \frac{G_F}{\sqrt{2}} V_{ud}^* V_{us} \sum_i C_i(\mu) \left(\frac{1}{\sqrt{3}} M_i^{K^+} \right). \quad (12)$$

The relative factor between the two expressions is due to the different Clebsch-Gordan coefficients.

A major challenge in the calculation of A_2 (and even more so in the calculation of A_0) is to ensure that the pions have physical momenta. In the centre-of-mass frame with periodic boundary conditions, the ground-state for the two-pion system has each pion at rest. The evaluation of matrix elements at physical kinematics therefore corresponds to the contribution from an excited two-pion state resulting in a considerable loss of precision. We can avoid the necessity of multi-exponential fits to extract the excited state contribution by utilizing the technique suggested in [11, 12] and applied successfully in our original calculation of A_2 [1, 2]: we introduce antiperiodic boundary conditions for the (valence) d quark in all three spatial directions, and periodic boundary conditions for the u and s quarks [11]. We then exploit the Wigner-Eckart theorem to relate $K^+ \rightarrow \pi^+ \pi^0$ matrix elements to those for the unphysical transition $K^+ \rightarrow \pi^+ \pi^+$. The relation is

$$\frac{1}{\sqrt{2}} \langle (\pi\pi)_{I_3=1}^{I=2} | Q_{\Delta I_3=1/2,i}^{\Delta I=3/2} | K^+ \rangle = \frac{3}{2} \frac{\langle (\pi\pi)_{I_3=2}^{I=2} | Q_{\Delta I_3=3/2,i}^{\Delta I=3/2} | K^+ \rangle}{\langle \pi^+ \pi^+ |}. \quad (13)$$

The indices I and I_3 label the two-pion state's total and third component of isospin respectively. With antiperiodic boundary conditions in three spatial directions, the $|\pi^+ \pi^+\rangle$ ground state has total momentum $\vec{0}$, with each pion having momentum $|\vec{p}_\pi| = \sqrt{3} \pi/L$. It can be seen from Tab.I that $E_{\pi\pi}$ is very close to m_K on both the 64^3 and 48^3 ensembles. (For the smaller physical volume in our original calculation [1, 2], we imposed antiperiodic boundary conditions for the d quark in two spatial directions in order to achieve $E_{\pi\pi} \simeq m_K$.) Note that with both periodic and antiperiodic boundary conditions on the d quark, the lowest momentum of the π^0 meson is zero; this motivates the use of the Wigner-Eckart theorem to reformulate the calculation to that of a matrix element with a $|\pi^+ \pi^+\rangle$ final state.

The operators $Q_{\Delta I_3=3/2}^{\Delta I=3/2}$ which appear on the right-hand side of Eq. (13), and which correspond to the $Q_{\Delta I_3=1/2}^{\Delta I=3/2}$ operators in Eqs. (8)-(10), are

$$Q_{(27,1)} = (\bar{s}_i d_i)_L (\bar{u}_j d_j)_L, \quad Q_{(8,8)} = (\bar{s}_i d_i)_L (\bar{u}_j d_j)_R, \quad Q_{(8,8)_{\text{mx}}} = (\bar{s}_i d_j)_L (\bar{u}_j d_i)_R. \quad (14)$$

To simplify the notation we have dropped the labels $\Delta I = 3/2$ and $\Delta I_z = 3/2$ on the operators in Eq. (14); this will be implicit in the following. In this paper we compute the $K \rightarrow \pi\pi$ matrix elements of the three operators in Eq. (14).

The factor of $3/2$ in Eq. (13) is a combination of $\sqrt{3}/2$ coming from the Clebsch-Gordan coefficients and the Wigner-Eckart theorem, and a further $\sqrt{3}$ corresponding to the simple choice for the normalization of operators in Eq. (14). The amplitude A_2 is given in terms of the $K^+ \rightarrow \pi^+ \pi^+$ matrix elements M_i by:

$$A_2 = \frac{G_F}{\sqrt{2}} V_{ud}^* V_{us} \frac{\sqrt{3}}{2} \sum_i C_i(\mu) M_i. \quad (15)$$

Since it is the $K^+ \rightarrow \pi^+ \pi^+$ matrix elements which we compute directly in this paper, we choose the compact notation $M_i \equiv M_i^{K^+ \rightarrow \pi^+ \pi^+}$. The label i runs over the three operators in Eq. (14).

A. Evaluation of the correlation functions

The bare matrix elements are obtained from the computation of two and three point correlation functions. The three-point functions are:

$$C_i^{K \rightarrow \pi\pi}(t_{\text{op}}) = \langle 0 | \sigma_{\pi\pi}(t_{\pi\pi}) Q_i(t_{\text{op}}) \sigma_K^\dagger(0) | 0 \rangle, \quad (16)$$

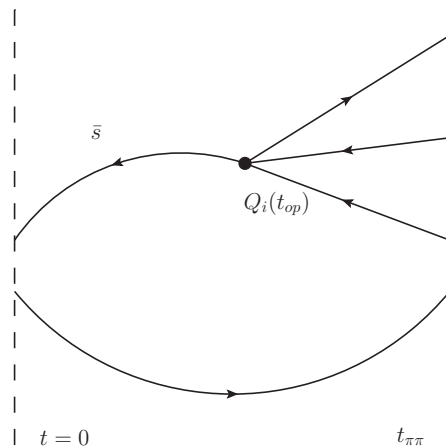


FIG. 3: Diagrammatic representation of the $K \rightarrow \pi\pi$ three-point function defined in Eq. (16). The strange quark propagator is explicitly labelled, the remaining lines represent light-quark propagators.

where Q_i is one of the three operators in Eq. (14) and σ_K and $\sigma_{\pi\pi}$ are interpolating operators for the kaon and two-pion state respectively. For σ_K and $\sigma_{\pi\pi}$ we take Coulomb gauge-fixed wall-source operators defined as follows:

$$\sigma_K(t) \equiv \sum_{\vec{x}_1, \vec{x}_2} \bar{s}(\vec{x}_1, t) \gamma^5 u(\vec{x}_2, t), \quad (17)$$

$$\sigma_{\pi\pi}(t) \equiv [\bar{d}(t)\gamma^5 u(t)] [\bar{d}(t)\gamma^5 u(t)], \quad (18)$$

where in (18) we have used the cosine momentum sources for the d quark:

$$d(t) = \sum_{x, y, z} d(x, y, z, t) \cos(xp_x) \cos(yp_y) \cos(zp_z). \quad (19)$$

$d(x, y, z, t)$ represents the d -quark field and the components of momenta satisfy $p_x = p_y = p_z = \pi/L$. Just as for the u -quark source in Eq. (17), the u -quark sources in $\sigma_{\pi\pi}$ shown in Eq. (18) are given zero momentum by summing them over the full spatial volume, evaluated in the Coulomb gauge. As explained in Ref. [2] the cosine source described above creates d quarks with both signs for each component of the three momentum $\pm p_i$, for $i = x, y$ and z . This will then produce pairs of pions with total momentum in each direction of $\pm 2\pi/L$ in addition to the desired value of $\vec{0}$. For the three-point functions described in Eq. (16), the zero total momentum of the decaying kaon and three-momentum conservation imply that the non-zero π - π momenta cannot occur. For the two-point function defined in Eq. (22) below we use a π - π sink which is different from the source and which explicitly projects onto π - π states with zero total momentum, as described in Ref. [2]. A further subtlety, not described in that reference, relates to the possible angular momentum of the two-pion state. For our two identical π^+ bosons which carry equal but opposite momenta, there are actually four possible states given our boundary conditions. Specifically, the π^+ which carries $p_x = +\pi/L$ may have four possible values for the other momentum components: $p_y = \pm\pi/L$ and $p_z = \pm\pi/L$. These four states form a four-dimensional representation of the cubic symmetry group, which decomposes into two irreducible representations: a singlet (A_1) and a triplet (T_2), out of which only A_1 contains an s-wave contribution. Since the lowest energy level of the finite volume $I = 2$ s-wave spectrum of the A_1 representation is nearly degenerate with the lowest energy level of the d-wave spectrum of the T_2 representation, it is important that we use the cubically symmetrical source specified in Eq. (19) which couples only to the A_1 state of interest.

The spinor and color labels are contracted within each set of square parentheses in Eq. (18). A schematic diagram of the correlation function $C_i^{K \rightarrow \pi\pi}(t_{\text{op}})$ is shown in Fig. 3.

We have evaluated $C_i^{K \rightarrow \pi\pi}(t_{\text{op}})$ for a range of values of the source-sink separations $t_{\pi\pi}$. For the 48^3 (64^3) ensemble we performed the calculations for values of $t_{\pi\pi}$ between 24 and 39 (26 and 36). These separations were chosen to be large enough for the plateau region to give a reliable fit and small enough for the around-the-world effects to be small. The fitting ranges were chosen to be from 10 to $t_{\pi\pi} - 10$ for both ensembles. These choices are motivated by the locations of plateau regions in Fig. 4.

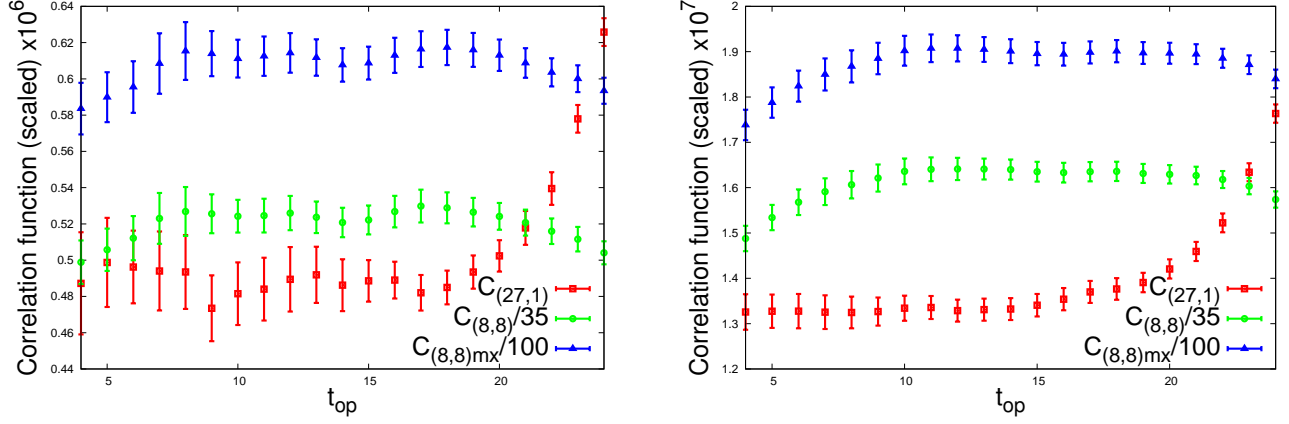


FIG. 4: $K \rightarrow \pi\pi$ three-point correlation function on the 48^3 lattice (left) and 64^3 lattice (right) with a kaon-pion separation of $t_{\pi\pi} = 26$.

For sufficiently large time separations t_{op} and $t_{\pi\pi} - t_{\text{op}}$, the expected time dependence of $C_i^{K \rightarrow \pi\pi}(t_{\text{op}})$ is:

$$C_i^{K \rightarrow \pi\pi}(t_{\text{op}}) = N_{\pi\pi} N_K M_i^{\text{bare}} e^{-(m_K - E_{\pi\pi})t_{\text{op}}} e^{-E_{\pi\pi}t_{\pi\pi}}, \quad (20)$$

where

$$N_{\pi\pi} = |\langle \pi\pi | \sigma_{\pi\pi}(0) | 0 \rangle| \quad \text{and} \quad N_K = |\langle K | \sigma_K(0) | 0 \rangle|. \quad (21)$$

We have introduced the label “bare” as a reminder that M_i^{bare} are matrix elements of the bare operators in the lattice regularization which we are using. The renormalization of the operators is discussed in the following section. For illustration, in Fig. 4 we plot $C_i^{K \rightarrow \pi\pi}(t_{\text{op}})$ computed on each of the two ensembles for $t_{\pi\pi} = 26$. The observed plateaus are a manifestation of the fact that the volumes have been tuned so that $E_{\pi\pi} \simeq m_K$ (cf. Eq. (20)).

We obtain the matrix elements M_i by fitting Eq. (20), using the values of $N_{\pi\pi}$, N_K , m_K and $E_{\pi\pi}$ obtained from fitting (under the jackknife) the correlation functions:

$$C_{\pi\pi}(t) = \langle 0 | \sigma_{\pi\pi}^\dagger(t, \vec{p} = 0) \sigma_{\pi\pi}(0) | 0 \rangle \quad \text{and} \quad C_K(t) = \langle 0 | \sigma_K(t) \sigma_K^\dagger(0) | 0 \rangle, \quad (22)$$

which have the following time dependence:

$$C_{\pi\pi}(t) \xrightarrow{t \rightarrow \infty} |N_{\pi\pi}|^2 \left(e^{-E_{\pi\pi}t} + e^{-E_{\pi\pi}(T-t)} + C \right), \quad (23)$$

$$C_K(t) \xrightarrow{t \rightarrow \infty} |N_K|^2 \left(e^{-m_K t} + e^{-m_K(T-t)} \right). \quad (24)$$

The ‘ $t \rightarrow \infty$ ’ limit should be understood as taking a sufficiently large time separation so that excited state contributions are negligible. Introducing the constant C in Eq. (23) allows one to account for possible around-the-world effects in $C_{\pi\pi}$.

As a check, we can also construct the time-independent ratio of the correlation functions:

$$\frac{C_{K \rightarrow \pi\pi}^i(t)}{C_K(t) C_{\pi\pi}(t_{\pi\pi} - t)} = \frac{M_i^{\text{bare}}}{N_{\pi\pi} N_K}. \quad (25)$$

This ratio is plotted for $t_{\pi\pi} = 26$ in Fig. 5. As anticipated, all three operators exhibit a constant behaviour in the region where the contribution from excited states is negligible. Eq. (25) is expected to hold in the region $0 \ll t \ll t_{\pi\pi} \ll T$, where T is the total time extent of the lattice. In this region ‘around-the-world’ effects arising from different time orderings of the operators can be neglected.

The values of the bare $K^+ \rightarrow \pi^+\pi^+$ matrix elements are shown in Tab. II. The entries have been obtained by performing weighted averages (under the jackknife) over the values obtained for each choice of $t_{\pi\pi}$.

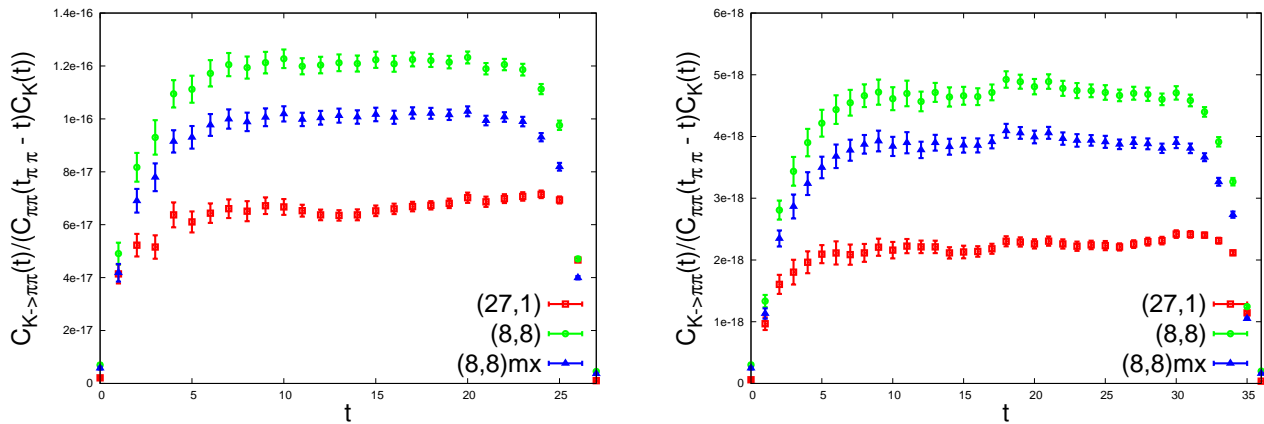


FIG. 5: Ratios of $K \rightarrow \pi\pi$ three-point correlation function to the two point functions (Eq. (25)) on the 48^3 lattice (left) and the 64^3 lattice (right) with a kaon-pion separations of $t_{\pi\pi} = 27$ and 36 respectively.

	$a^3 M_{(27,1)}^{\text{bare}}$	$a^3 M_{(8,8)}^{\text{bare}}$	$a^3 M_{(8,8)\text{mx}}^{\text{bare}}$
48^3 ensemble	$7.400(70) \times 10^{-5}$	$9.171(69) \times 10^{-3}$	$3.058(23) \times 10^{-2}$
64^3 ensemble	$2.742(22) \times 10^{-5}$	$3.942(39) \times 10^{-3}$	$1.308(13) \times 10^{-2}$

TABLE II: Results for the bare $K^+ \rightarrow \pi^+ \pi^+$ matrix elements in lattice units. Only statistical errors are shown.

IV. RENORMALIZATION OF THE OPERATORS

Having determined the matrix elements of the bare operators in the lattice regularization we now have to combine them with the remaining factors in Eq. (6) to obtain A_2 . The Wilson coefficients ($C_i(\mu)$) and composite operators ($Q_i(\mu)$) appearing in Eq. (6) are separately renormalization scheme and scale (μ) dependent. To obtain the physical amplitudes they must be combined in the same scheme and at the same scale. The $C_i(\mu)$ are calculated in perturbation theory for which it is convenient to use the $\overline{\text{MS}}$ -NDR scheme (called $\overline{\text{MS}}$ in the following). The matrix elements calculated in Sec. III, on the other hand, were obtained using bare operators with the lattice spacing as the ultraviolet regulator with the lattice discretization of QCD. The operators can be renormalized non-perturbatively, but only into schemes for which the renormalization condition can be imposed on lattice Green's functions. The $\overline{\text{MS}}$ scheme, which is based on dimensional regularization cannot be simulated in a lattice computation. Our procedure is to start by renormalizing the operators non-perturbatively into schemes which can be simulated, specifically the RI-SMOM schemes [13] as described in detail in [2] and briefly summarized below. The matching between the RI-SMOM and $\overline{\text{MS}}$ schemes is necessarily performed in perturbation theory and is currently known at one-loop order. (Below we also present the matrix elements in two RI-SMOM schemes so that if the perturbative coefficients are calculated to higher order in the future, these matrix elements can be used to reduce the systematic uncertainty in A_2 due to the truncation of the perturbation series.)

We now briefly summarise the renormalization procedure. We write the five-point amputated Green's functions of the three operators in Eq. (14) as a three-component vector $\Lambda = (\Lambda_{(27,1)}, \Lambda_{(8,8)}, \Lambda_{(8,8)\text{mx}}) \equiv (\Lambda_1, \Lambda_2, \Lambda_3)$, and impose a renormalization condition of the form

$$P \{ \Lambda^R(\mu) \} = F, \quad (26)$$

where P is a vector of projectors and F the corresponding tree-level matrix. Denoting the tree-level contribution by the superscript (0) and including explicitly the spinor and color labels, the matrix F is given by

$$P_i \{ \Lambda_j^{(0)} \} \equiv [P_i]_{\beta\alpha;\delta\gamma}^{BA;DC} \left[\Lambda_j^{(0)} \right]_{\alpha\beta;\gamma\delta}^{AB;CD} = F_{ij}. \quad (27)$$

Here Greek letters label spinor components, the upper-case Roman letters represent color indices and $i, j = 1, 2, 3$

denote the operators and projectors. For illustration, the tree-level value of the Green's function of $Q^{(27,1)}$ is

$$\begin{aligned} \left[\Lambda_1^{(0)} \right]_{\alpha\beta;\gamma\delta}^{AB;CD} &= [(\gamma^\mu)_{\alpha\beta}(\gamma^\mu)_{\gamma\delta} + (\gamma^\mu\gamma_5)_{\alpha\beta}(\gamma^\mu\gamma_5)_{\gamma\delta}] \delta^{AB}\delta^{CD} \\ &\quad - [(\gamma^\mu)_{\alpha\delta}(\gamma^\mu)_{\gamma\beta} + (\gamma^\mu\gamma_5)_{\alpha\delta}(\gamma^\mu\gamma_5)_{\gamma\beta}] \delta^{AD}\delta^{BC}. \end{aligned} \quad (28)$$

For the renormalization we only consider the parity-even component of the four-quark operators.

The choice of projectors is not unique and we implement two different sets known as the γ_μ and \not{q} -projectors, given explicitly by

$$\left[P^{(\gamma^\mu)} \right]_{\beta\alpha;\delta\gamma}^{JI;LK} = \begin{pmatrix} [(\gamma^\mu)_{\beta\alpha}(\gamma^\mu)_{\delta\gamma} + (\gamma^\mu\gamma_5)_{\beta\alpha}(\gamma^\mu\gamma_5)_{\delta\gamma}] \delta^{JI}\delta^{LK} \\ [(\gamma^\mu)_{\beta\alpha}(\gamma^\mu)_{\delta\gamma} - (\gamma^\mu\gamma_5)_{\beta\alpha}(\gamma^\mu\gamma_5)_{\delta\gamma}] \delta^{JI}\delta^{LK} \\ [(\gamma^\mu)_{\beta\gamma}(\gamma^\mu)_{\delta\alpha} - (\gamma^\mu\gamma_5)_{\beta\gamma}(\gamma^\mu\gamma_5)_{\delta\alpha}] \delta^{JK}\delta^{LI} \end{pmatrix} \quad (29)$$

and

$$\left[P^{(\not{q})} \right]_{\beta\alpha\beta;\delta\gamma}^{JI;LK} = \begin{pmatrix} [(\not{q})_{\beta\alpha}(\not{q})_{\delta\gamma} + (\not{q}\gamma_5)_{\beta\alpha}(\not{q}\gamma_5)_{\delta\gamma}] \delta^{JI}\delta^{LK} \\ [(\not{q})_{\beta\alpha}(\not{q})_{\delta\gamma} - (\not{q}\gamma_5)_{\beta\alpha}(\not{q}\gamma_5)_{\delta\gamma}] \delta^{JI}\delta^{LK} \\ [(\not{q})_{\beta\gamma}(\not{q})_{\delta\alpha} - (\not{q}\gamma_5)_{\beta\gamma}(\not{q}\gamma_5)_{\delta\alpha}] \delta^{JK}\delta^{LI} \end{pmatrix}. \quad (30)$$

The corresponding matrices F read

$$F^{(\gamma^\mu)} = \begin{pmatrix} 128N(N+1) & 0 & 0 \\ 0 & 128N^2 & 128N \\ 0 & 128N & 128N^2 \end{pmatrix} \quad (31)$$

and

$$F^{\not{q}} = q^2 \begin{pmatrix} 32N(N+1) & 0 & 0 \\ 0 & 32N^2 & 32N \\ 0 & 32N & 32N^2 \end{pmatrix}, \quad (32)$$

where $N = 3$ is the number of colors.

The final result for the amplitude is, of course, independent of the choice of intermediate scheme defined by P , but comparing the results obtained with different projection operators gives us an estimate of the systematic uncertainty due to the truncation of perturbation theory in relating the RI-SMOM schemes to the $\overline{\text{MS}}$ schemes.

The renormalized operators are related to the bare ones by a matrix relation of the form:

$$Q_i^{\text{R}}(\mu) = Z_{ij}(\mu a) Q_j^{\text{bare}}(a). \quad (33)$$

In order to extract the renormalization constants we follow the standard procedure [14, 15] and compute numerically the amputated Green's functions of the bare operators in Eq. (14) with particular choices of external momenta (as discussed below) on Landau gauge-fixed configurations. We next solve equation (26) which we rewrite in the form

$$\frac{Z_{ij}(\mu a)}{Z_q^2(\mu a)} P_k \{ (\Lambda_j^{\text{bare}}(a)) \}_{\mu^2=p^2} = F_{ik}, \quad (34)$$

where $\sqrt{Z_q}$ is the quark field renormalization constant and μ is the renormalization scale, which we ultimately choose to be 3 GeV.

The choice of Z_q is also not unique, and we use the following two cases:

$$\frac{Z_q^{(\not{q})}}{Z_V} = \frac{q^\mu}{12q^2} \text{Tr} \Lambda_V^\mu \not{q}, \quad \text{and} \quad \frac{Z_q^{(\gamma^\mu)}}{Z_V} = \frac{1}{48} \text{Tr} \Lambda_V^\mu \gamma^\mu, \quad (35)$$

where Λ_V^μ is the three-point amputated Green's function of the local vector current and Z_V is the renormalization constant of the local vector current. In practice, we multiply each side of Eq. (34) by the square of the corresponding side of Eq. (35). This eliminates Z_q and after this multiplication the left-hand side of Eq. (34) contains the ratio of

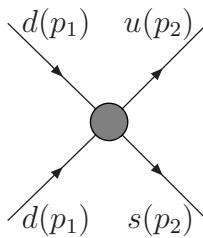


FIG. 6: Momentum flow defining a renormalization condition of a four quark operator in RI-SMOM scheme. The momenta are chosen so that $p_1^2 = p_2^2 = (p_1 - p_2)^2 \equiv \mu^2$.

renormalization factors Z_{ij}/Z_V^2 . Z_V is then calculated by imposing the Ward identity $Z_V \langle P | V^4 | P \rangle = 2m_P$, where V^μ is the local vector current and $|P\rangle$ is the state of a pseudoscalar meson P at rest with mass m_P ; this is explained in detail in [7].

The choice of projection operator for the four-quark operator and Z_q defines a renormalization scheme, which we will label (a, b) with $a, b \in \gamma^\mu, \not{q}$ for the choice of $P^{(a)}$ and $Z_q^{(b)}$. In particular, we consider the (γ^μ, γ^μ) and (\not{q}, \not{q}) schemes, having found in earlier studies that the perturbative conversion to the $\overline{\text{MS}}$ scheme is more precise in these schemes. This is based on the observation that the non-perturbative running is generally closer to the perturbative one for these schemes for the four-quark operators in Eq. (14) [2, 16]. As explained below, we follow our previous practice and choose the (\not{q}, \not{q}) scheme for our central value and the (γ^μ, γ^μ) scheme to estimate the error due to the perturbative conversion to the $\overline{\text{MS}}$ scheme.

Chiral symmetry suppresses mixing of operators in different irreducible representations of the chiral symmetry group, so that if the symmetry is exact, Z_{ij} is a block diagonal matrix with a 1×1 block corresponding to the renormalization of the $(27, 1)$ operator and 2×2 block corresponding to the mixing of $(8, 8)$ and $(8, 8)_{\text{mix}}$ operators. In a massless renormalization scheme with a chiral discretization such as the Domain Wall action, we expect a mixing pattern very similar to this, but with a small $O((am_{\text{res}})^2)$ mixing between the blocks.

The mixing of the operator $Q_{(27,1)}$ with either of $Q_{(8,8)}$ or $Q_{(8,8)_{\text{mix}}}$ due to explicit chiral symmetry breaking induced by finite L_s is proportional to $(am_{\text{res}})^2$ (which is $\lesssim 3.6 \times 10^{-7}$ in this work). Such mixing can result from two mechanisms [17, 18]. First, both quarks in a left-handed $\bar{q}q$ pair in $Q_{(27,1)}$ can propagate in the fifth dimension from the left-hand to the right-hand wall, exploiting numerous but exponentially damped modes which even in perturbation theory link the left- and right-hand walls. This will change the $(27, 1)$ operator into one transforming as the $(8, 8)$ representation, but requires the propagation of two quarks from the left-hand to the right-hand wall. This incurs a penalty of $(am_{\text{res}})^2$ since one power of the residual mass results from the fifth-dimensional mixing of the left- and right-handed components of a single quark.

The second mechanism is non-perturbative and more subtle. For this case the propagation results from the left-right tunneling that can be caused by an eigenvector of the 5-dimensional transfer matrix with a near-unit eigenvalue. Such eigenvectors permit $O(1)$ left-right mixing but are rare and therefore give a small contribution to m_{res} . Under some circumstances such modes can simultaneously allow a number of quark flavors to flip chirality. However, to change a $(27, 1)$ representation into an $(8, 8)$ one, both a quark and an anti-quark must flip chirality which requires two distinct transfer matrix eigenvectors and is therefore also doubly suppressed by a factor $(am_{\text{res}})^2$. Such doubled suppression will not occur for the mixing between the operator $Q_{(27,1)}$ and, for example, an operator in the $(\bar{6}, 6)$ representation. Here a single transfer matrix eigenvector with near-unit eigenvalue can result in a $O(am_{\text{res}})$ mixing between $Q_{(27,1)}$ and $(\bar{3}(1 + \gamma^5)d)(\bar{u}(1 + \gamma^5)d)$ by allowing both a u - and a d -quark (localized near this eigenvector) to flip chirality. This kind of mixing has been studied for example in [19] and it was found to be largely suppressed by our choice of kinematics, as explained below.

In order to suppress physical infrared chiral-symmetry breaking effects we choose to impose the renormalization conditions with the kinematics indicated in Fig. 6 with $p_1^2 = p_2^2 = (p_1 - p_2)^2 \equiv \mu^2$. We compute the Green's functions for several momenta and interpolate to $\mu = 3 \text{ GeV}$ using a quadratic ansatz. Using partially twisted boundary conditions, we have a good resolution around the targeted momentum. The momenta in such RI-SMOM schemes are chosen so that there are no “exceptional” channels, i.e. no channels in which the square of the momenta is small [13]. (This is in contrast with the original RI-MOM scheme [14, 15] in which $p_1 = p_2$.) We have already checked that with Domain-Wall fermions and this choice of kinematics the chirally forbidden matrix elements are numerically negligible [2]. In the present computation, we use the 48^3 and 64^3 ensembles which have physical light and strange sea-quark masses. However, the light quark mass is used in all of the valence quarks propagators in the five-point Green's functions, including those for both light and strange quarks. We do not extrapolate either the sea or valence

	48 ³ Ensembles	64 ³ Ensembles
Re(A_2) (γ^μ, γ^μ)	1.346(11) _{stat} (1) _{NPR} $\times 10^{-8}$ GeV	1.4029(93) _{stat} (11) _{NPR} $\times 10^{-8}$ GeV
Im(A_2) (γ^μ, γ^μ)	-5.739(46) _{stat} (8) _{NPR} $\times 10^{-13}$ GeV	-6.143(73) _{stat} (9) _{NPR} $\times 10^{-13}$ GeV
Re(A_2) (\not{q}, \not{q})	1.386(12) _{stat} (1) _{NPR} $\times 10^{-8}$ GeV	1.4386(95) _{stat} (11) _{NPR} $\times 10^{-8}$ GeV
Im(A_2) (\not{q}, \not{q})	-6.174(49) _{stat} (9) _{NPR} $\times 10^{-13}$ GeV	-6.548(78) _{stat} (10) _{NPR} $\times 10^{-13}$ GeV

TABLE III: The amplitude A_2 calculated using two different intermediate RI-SMOM schemes. The two errors, labelled by “stat” and “NPR”, are the statistical uncertainties in the evaluation of the bare matrix elements and Z_{ij} respectively. Discrepancies in the results in the two schemes are attributed to the truncation in the matching to the $\overline{\text{MS}}$ scheme.

quark masses to zero and, strictly speaking, do not work in the chiral limit. In practice the light quark masses are sufficiently small that their effects are negligible as is the non-zero mass of the strange sea quark. Comparing our results with those of our previous work (with Shamir domain wall fermions) where a chiral extrapolation was performed we find agreement at the per-mille level or better.

We find that all the chirally forbidden renormalization factors are smaller than 10^{-5} , so we set the corresponding matrix elements of $P_i\{\Lambda_j\}$ to zero and finally obtain the renormalization matrices:

$$Z_{\beta=2.13}^{(\gamma^\mu, \gamma^\mu)}(\mu = 3 \text{ GeV}) = \begin{pmatrix} 0.4617(3) & 0 & 0 \\ 0 & 0.5302(4) & -0.07018(6) \\ 0 & -0.0386(1) & 0.4451(5) \end{pmatrix} \quad (36)$$

$$Z_{\beta=2.13}^{(\not{q}, \not{q})}(\mu = 3 \text{ GeV}) = \begin{pmatrix} 0.4822(3) & 0 & 0 \\ 0 & 0.5305(4) & -0.07135(7) \\ 0 & -0.0637(1) & 0.5052(6) \end{pmatrix} \quad (37)$$

for the 48³ ensembles and

$$Z_{\beta=2.25}^{(\gamma^\mu, \gamma^\mu)}(\mu = 3 \text{ GeV}) = \begin{pmatrix} 0.5194(2) & 0 & 0 \\ 0 & 0.5774(2) & -0.0751(1) \\ 0 & -0.02797(7) & 0.4431(6) \end{pmatrix} \quad (38)$$

$$Z_{\beta=2.25}^{(\not{q}, \not{q})}(\mu = 3 \text{ GeV}) = \begin{pmatrix} 0.5399(2) & 0 & 0 \\ 0 & 0.5782(2) & -0.0761(1) \\ 0 & -0.05230(4) & 0.4990(5) \end{pmatrix} \quad (39)$$

for the 64³ ensembles. With momentum sources [20], only few configurations are needed to obtain an excellent statistical precision. The number of Landau gauge-fixed configurations used to obtain these results varies between 5 and 15. The statistical errors were estimated with 200 bootstrap samples. The matrices in Eqs. (36)–(39) are the ones used in Eq. (33) to obtain the operators renormalized in the RI-SMOM schemes at the scale $\mu = 3 \text{ GeV}$ from the corresponding lattice bare operators.

The procedure described above enables us to calculate the matrix elements of the operators in Eq. (14) in the (continuum) RI-SMOM schemes with a very small systematic uncertainty due to the renormalization. The Wilson coefficients however, are computed in the $\overline{\text{MS}}$ scheme and so we have to match the RI-SMOM schemes to the $\overline{\text{MS}}$ one. We repeat that this matching is perturbative and at present is only known to one-loop order [21]; this limitation amplifies the uncertainty due to the renormalization. This uncertainty could be reduced by extending the perturbative calculations to higher orders. Future lattice calculations could also help here by using step scaling to run the renormalization constants obtained in the RI-SMOM schemes non-perturbatively to larger momentum scales. The perturbative matching to the $\overline{\text{MS}}$ scheme can then be performed at these larger scales where the coupling constant is smaller, leading to smaller uncertainties. We now estimate the current uncertainty due to the matching.

To estimate the uncertainty due to the truncation of the perturbative matching factors, we note that the matrix elements in the $\overline{\text{MS}}$ scheme should be independent of the choice of intermediate RI-SMOM scheme. Differences in

	$E_{\pi\pi}$	q	δ [radians]	$\frac{\partial\delta}{\partial q}$	$\frac{\partial\phi}{\partial q}$
48^3	0.2873(13)	0.9087(61)	-0.158(22)	-0.174(24)	3.7147(20)
64^3	0.21512(68)	0.9157(43)	-0.184(16)	-0.201(17)	3.7171(15)

TABLE IV: Contributions to the Lellouch-Lüscher factor on the 48^3 and 64^3 ensembles. The rate of change of the phase shift was calculated by using a linear approximation in momentum as explained in the text.

the results are observed (see Tab. III) and attributed to the truncation. Following the procedure in [1, 2] we take the result obtained using the (\not{q}, \not{q}) intermediate scheme as our central value and the difference of the results obtained using the two schemes as an estimate of the systematic error. This uncertainty is marked as ‘‘NPR (perturbative)’’ in the error budgets presented in Tabs. IX and X in Sec. VI. The uncertainties marked as ‘‘NPR (nonperturbative)’’ are the statistical errors in the evaluation of Z_{ij} .

V. FINITE VOLUME EFFECTS

The presence of two pions in the final state in $K \rightarrow \pi\pi$ decays leads to finite-volume corrections which decrease as inverse powers of the volume, in addition to the exponential correction present in simpler quantities such as decay constants and form factors. The power corrections result in a multiplicative correction to the matrix element [22]:

$$\langle \pi\pi | H_W | K \rangle_\infty = F \langle \pi\pi | H_W | K \rangle_{FV}. \quad (40)$$

The subscripts ∞ and FV correspond to infinite and finite volume respectively, and the factor F is given by the Lellouch-Lüscher formula [22]:

$$F^2 = 8\pi q \left(\frac{\partial\phi}{\partial q} + \frac{\partial\delta}{\partial q} \right) \frac{m_K E_{\pi\pi}^2}{p^3}, \quad (41)$$

where p is the magnitude of the momentum of a pion in the centre of mass frame given by $p = \sqrt{\frac{E_{\pi\pi}^2}{4} - m_\pi^2}$ and q is defined as $q = pL/2\pi$. Since the π^+ mesons satisfy anti-periodic boundary conditions in all three spatial directions, the function ϕ in this case is defined by the condition:

$$\tan \phi = -\frac{q\pi^{3/2}}{Z_{00}(1; q)}, \quad Z_{00}(1; q) = \frac{1}{\sqrt{4\pi}} \sum_{n \in \mathbb{Z}^3} \frac{1}{(n + (\frac{1}{2}, \frac{1}{2}, \frac{1}{2}))^2 - q^2}. \quad (42)$$

δ is the two-pion s-wave phase shift, which can be calculated using the Lüscher quantization condition, $\delta(q) + \phi(q) = n\pi$, but the calculation of the derivative in Eq. (41) requires an approximation.

The results presented in Tab. IV were obtained using the approximation that δ is a linear function of the momentum between 0 and p . Since the second term in the parentheses on the right-hand side of Eq. (41) is much smaller than the first and given the remaining systematic uncertainties discussed in Sec. VI, this procedure gives an adequate approximation. In order to estimate the error due to this approximation we also evaluate the derivative $\frac{\partial\delta}{\partial p}$ using the phenomenological curve of Ref. [23] illustrated in Fig. 7; we take the difference of the two procedures as an estimate of the corresponding uncertainty. For our central value we use the linear approximation for the derivative of the phase shift so that it is independent of phenomenological estimates.

At the pion momentum which corresponds to the decay of a physical kaon to two pions ($p = 207$ MeV) the value of the derivative of the phase shift with respect to the momentum obtained from the phenomenological curve is $9.53 \times 10^{-4} \text{ MeV}^{-1}$. Converting this to $\frac{\partial\delta}{\partial q}$ gives -0.216 for the 48^3 and -0.221 for the 64^3 ensembles. While this makes a significant difference to the derivative of the phase shift, it represents a relatively small uncertainty in the Lellouch-Lüscher factor $F \propto \frac{\partial\delta}{\partial q} + \frac{\partial\phi}{\partial q}$. This sum is dominated by the $\frac{\partial\phi}{\partial q}$ term and thus the difference in the Lellouch-Lüscher factor between both approaches to calculating $\frac{\partial\delta}{\partial q}$ amounts to 1.1% and 0.6% on the 48^3 and 64^3 ensembles respectively.

When quoting our central value we include the Lellouch-Lüscher factor evaluated as described in the preceding paragraph. In order to estimate the size of the remaining exponential finite-volume effects we use chiral perturbation theory and include the corresponding effects in our systematic uncertainty. Since we are only calculating an estimate,

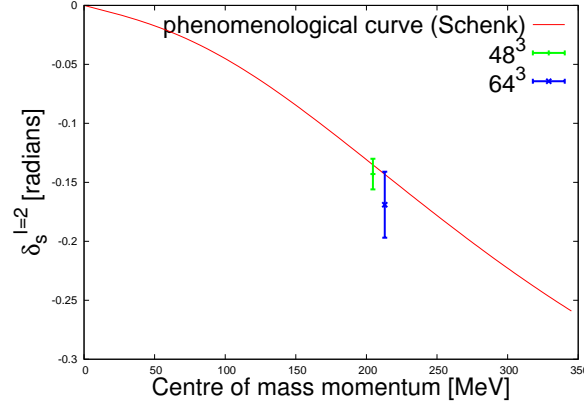


FIG. 7: Comparison of $I = 2$ two-pion s-wave phase shifts calculated using Lüscher's formula with the phenomenological curve from Ref. [23]. The computed results are consistent with the phenomenological curve.

we do not use partially-twisted chiral perturbation theory, but take both the sea and valence d -quarks to satisfy anti-periodic boundary conditions.

In $SU(3)_L \times SU(3)_R$ chiral perturbation theory, the leading order (LO) and leading logarithmic next-to-leading order (log) contributions to the (27,1) and (8,8) matrix elements are given by [6, 24]:

$$\mathcal{M}_{\text{LO}}^{27} = \langle \pi^+ \pi^- | \mathcal{O}^{(27,1),3/2} | K^0 \rangle_{\text{LO}} = -\frac{4i\alpha_{27}}{f_K f_\pi^2} (m_K^2 - m_\pi^2), \quad (43)$$

$$\begin{aligned} \mathcal{M}_{\text{log}}^{27} &= \langle \pi^+ \pi^- | \mathcal{O}^{(27,1),3/2} | K^0 \rangle_{\text{log}} \\ &= -\frac{4i\alpha_{27}}{f_K f_\pi^2} \frac{1}{f^2} \left[-\frac{1}{12} m_K^4 \left(1 - \frac{m_K^2}{m_\pi^2} \right) \beta(m_\pi^2, m_K^2, m_\eta^2) + m_K^2 \left(\frac{5 m_K^4}{4 m_\pi^2} \right. \right. \\ &\quad \left. \left. - \frac{13}{4} m_K^2 + 2m_\pi^2 \right) \beta(m_\pi^2, m_K^2, m_\pi^2) + (m_K^4 - 3m_\pi^2 m_K^2 + 2m_\pi^4) \right. \\ &\quad \left. \times \beta(m_K^2, m_\pi^2, m_\pi^2) + \left(-\frac{1}{4} \frac{m_K^4}{m_\pi^2} - \frac{1}{12} m_K^2 + \frac{1}{3} m_\pi^2 \right) \ell(m_\eta^2) + \left(\frac{-m_K^4}{m_\pi^2} \right. \right. \\ &\quad \left. \left. - 4m_K^2 + 4m_\pi^2 \right) \ell(m_K^2) + \left(\frac{5 m_K^4}{4 m_\pi^2} - \frac{45}{4} m_K^2 + 11m_\pi^2 \right) \ell(m_\pi^2) \right], \quad (44) \end{aligned}$$

$$\mathcal{M}_{\text{LO}}^{88} = \langle \pi^+ \pi^- | \mathcal{O}^{(8,8),3/2} | K^0 \rangle_{\text{LO}} = -\frac{4i\alpha_{88}}{f_K f_\pi^2}, \quad (45)$$

$$\begin{aligned} \mathcal{M}_{\text{log}}^{88} &= \langle \pi^+ \pi^- | \mathcal{O}^{(8,8),3/2} | K^0 \rangle_{\text{log}} \\ &= -\frac{4i\alpha_{88}}{f_K f_\pi^2} \frac{1}{f^2} \left[\left(\frac{5 m_K^4}{4 m_\pi^2} - 2m_K^2 \right) \beta(m_\pi^2, m_K^2, m_\pi^2) + (m_K^2 - 2m_\pi^2) \right. \\ &\quad \left. \times \beta(m_K^2, m_\pi^2, m_\pi^2) + \frac{1}{4} \frac{m_K^4}{m_\pi^2} \beta(m_\pi^2, m_K^2, m_\eta^2) - \left(4 + \frac{1}{2} \frac{m_K^2}{m_\pi^2} \right) \ell(m_K^2) \right. \\ &\quad \left. + \left(\frac{5 m_K^2}{4 m_\pi^2} - 8 \right) \ell(m_\pi^2) - \frac{3}{4} \frac{m_K^2}{m_\pi^2} \ell(m_\eta^2) \right]. \quad (46) \end{aligned}$$

At this order m_η is given by the Gell-Mann-Okubo relation: $3m_\eta^2 = 4m_K^2 - m_\pi^2$.

The functions $\ell(m^2)$ and $\beta(q^2, m_1^2, m_2^2)$ correspond to diagrams with one and two pseudo-Goldstone boson propagators respectively as illustrated in Fig. 8 and they are the only sources of finite-volume corrections. They are given

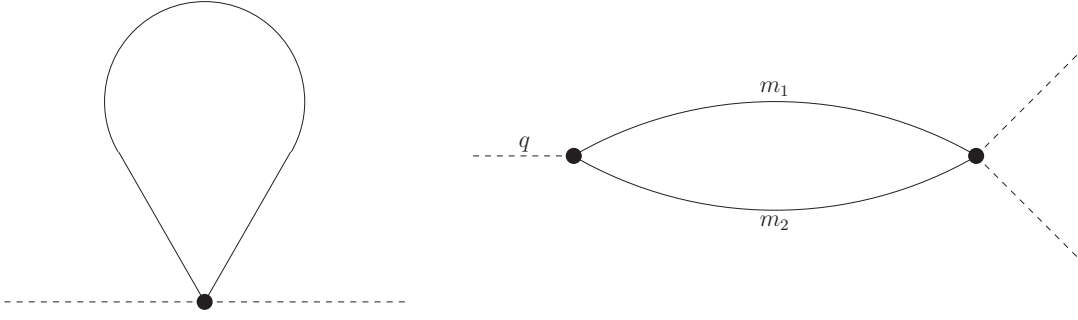


FIG. 8: Sample loop diagrams which contribute to finite-volume corrections of (27,1) and (8,8) $K \rightarrow \pi\pi$ matrix elements in chiral perturbation theory.

by (in Minkowski spacetime):

$$\ell(m^2) \equiv \not\int \int \frac{dk^0}{2\pi} \frac{i}{k^2 - m^2 + i\epsilon} = \not\int \frac{1}{\sqrt{\vec{k}^2 + m^2}}, \quad (47)$$

$$\beta(q, m_1, m_2) \equiv \not\int \int \frac{dk^0}{2\pi} \frac{i}{(k^2 - m_1^2)((q+k)^2 - m_2^2)} = \not\int \frac{\omega_1 + \omega_2}{2\omega_1\omega_2(q_0^2 - (\omega_1 + \omega_2)^2)}, \quad (48)$$

where the symbol $\not\int$ denotes the summation over \vec{k} in finite volume or the integration in infinite volume. $\omega_1 = \sqrt{\vec{k}^2 + m_1^2}$ and $\omega_2 = \sqrt{(\vec{q} - \vec{k})^2 + m_2^2}$. The difference between the sum and the integral can be calculated using the Poisson summation formula:

$$\frac{1}{L^3} \sum_{\vec{k}} f(\vec{k}) = \int \frac{d^3\vec{k}}{(2\pi)^3} f(\vec{k}) + \sum_{\vec{n} \neq \vec{0}} \int \frac{d^3\vec{k}}{(2\pi)^3} f(\vec{k}) e^{iL\vec{k} \cdot \vec{n}}, \quad (49)$$

where the summation on the left-hand side is over all $\vec{k} = \frac{2\pi}{L}\vec{n}$, where \vec{n} is a vector of integers. If f is a function that has no singularities on the real axis, then the second term on the right-hand side gives the exponential finite-volume corrections which we are trying to evaluate.

A. Corrections to $\ell(m^2)$

With periodic boundary conditions, applying the Poisson summation formula (49) to ℓ , writing \vec{k} in spherical polar coordinates and integrating over the angles, we obtain for the difference between the finite and infinite-volume values of $\ell(m^2)$ [25]

$$\Delta\ell(m, L) \equiv \frac{m^2}{16\pi^2} \delta_1(mL) \equiv \frac{m}{4\pi^2 L} \sum_{\vec{n} \neq \vec{0}} \frac{K_1(|\vec{n}|mL)}{|\vec{n}|}, \quad (50)$$

where K_1 is a modified Bessel function of the second kind, \vec{n} is an vector of integers and the sum is over all $\vec{n} \neq (0, 0, 0) \in \mathbb{Z}^3$.

Since our choice of boundary conditions breaks the isospin symmetry Eq. (50) does not give the correct finite-volume corrections for all the instances of ℓ which appear in Eqs. (44) and (46). Specifically, π^0 , K^+ and η satisfy periodic boundary conditions (so that the corresponding finite-volume corrections are indeed given by Eq. (50)) whereas π^\pm and K^0 satisfy antiperiodic boundary conditions for which the finite-volume corrections to ℓ are different. In the antiperiodic case, we replace $f(\vec{k})$ in Eq. (49) by $f(\vec{k} + \vec{q})$, where $\vec{q} = (\frac{\pi}{L})(1, 1, 1)$. Shifting the integration variable from \vec{k} to $\vec{k} + \vec{q}$, we find that $\delta_1(mL)$ in Eq. (50) is now replaced by:

$$\delta_1^A(mL) = \frac{4}{mL} \sum_{\vec{n} \neq \vec{0}} (-1)^{n_x + n_y + n_z} \frac{K_1(|\vec{n}|mL)}{|\vec{n}|}, \quad (51)$$

where the index A denotes that the correction is evaluated for a volume with antiperiodic boundary conditions in all spatial directions. The difference from the periodic case is the additional factor $(-1)^{n_x+n_y+n_z}$ in the summands. The known formulae in Eqs. (44) and (46) do not differentiate between different isospin components, and therefore do not specify which linear combination of periodic and antiperiodic corrections should be used. Since we are only using these formulae for an approximate estimate of the size of the error, we choose to be conservative and to include the larger corrections which are those obtained with the periodic boundary conditions given in Eqs. (50). The numerical results are presented in Tab. V and as expected the leading contributions come from the loops with a pion propagator.

B. Corrections to $\beta(m_\pi, m_K, m_\pi)$ and $\beta(m_\pi, m_K, m_\eta)$

We now consider the contributions from loops with two meson propagators and which are proportional to the function β . We start by discussing the corrections to $\beta(m_\pi, m_K, m_\pi)$ and $\beta(m_\pi, m_K, m_\eta)$, for which in Minkowski space the external energy is below the corresponding two-particle cut; e.g. in $\beta(m_\pi, m_K, m_\pi)$ the external energy in the centre-of-mass frame is m_π which is clearly smaller than $m_K + m_\pi$. In such situations the finite-volume corrections are exponentially small. We postpone the discussion of the contribution which does contain the two-particle cut, that proportional to $\beta(m_K, m_\pi, m_\pi)$, until the following subsection.

The corrections to $\beta(m_\pi, m_K, m_\pi)$ and $\beta(m_\pi, m_K, m_\eta)$ are proportional to

$$\Delta\beta(q, m_1, m_2) = \sum_{\vec{n} \neq 0} \int \frac{d^3\vec{k}}{(2\pi^3)} \frac{e^{i\vec{k}\cdot\vec{n}}(\omega_1 + \omega_2)}{2\omega_1\omega_2(q^2 - (\omega_1 + \omega_2)^2)} \quad (52)$$

with

$$\omega_1^2 = |\vec{k}|^2 + m_1^2 \quad \text{and} \quad \omega_2^2 = |\vec{q} + \vec{k}|^2 + m_2^2. \quad (53)$$

Because of the angular dependence inside the integrals, we evaluate the integrals numerically. With the boundary conditions which we are using the corrections with a K^+ and π^- are equal and opposite to those with the neutral mesons. In the estimate of the uncertainty we conservatively do not exploit the cancellation but take the absolute value in each case.

We note that care must be taken when using Eqs. (71) and (73) for the finite-volume corrections to β in Sec. VIII of [6]. In Eq. (52) above, the two terms in the factor in the denominator of the integrand $q^2 - (\omega_1 + \omega_2)^2$ come with opposite signs. How this arises in finite-volume Euclidean correlation functions is explained in Appendix A following [5]. The corresponding terms in the denominator of Eq. (73) in [6] appear (incorrectly) with the same sign.

C. $\beta(m_K, m_\pi, m_\pi)$

Kinematically this case is simpler than the two β integrals which were evaluated in Sec. VB since the external particle (K) is now at rest which eliminates the angular dependence from the integral. Furthermore, both internal π^+ propagators satisfy antiperiodic boundary conditions. In this case however, the integral for β has a pole at $\omega_\pi = m_K/2$, so the Poisson summation formula will give both the exponential and power-like corrections. The power corrections are included as the Lellouch-Lüscher factor F in Eq. (40) and we do not include these in the estimate of the finite-volume uncertainty. The evaluation of the remaining exponential corrections following the approach of [26] is explained in Appendix A.

Quantity	48 ³ Lattice	64 ³ Lattice
L	5.48 fm	5.36 fm
$\Delta l(m_\pi^2)$	14.32 MeV ²	16.39 MeV ²
$\Delta l(m_K^2)$	(9.05×10^{-4}) MeV ²	(1.03×10^{-3}) MeV ²
$\Delta l(m_\eta^2)$	(1.32×10^{-4}) MeV ²	(1.52×10^{-4}) MeV ²
$\Delta\beta(m_\pi, m_K, m_\eta)$	3.0×10^{-7}	3.0×10^{-7}
$\Delta\beta(m_\pi, m_K, m_\pi)$	5.0×10^{-5}	5.2×10^{-5}
$\Delta\beta(m_K, m_\pi, m_\pi)$	6.67×10^{-5}	6.97×10^{-5}
$\frac{\Delta M_{(27,1)}}{M_{(27,1)}}$	0.022	0.024
$\frac{\Delta M_{(8,8)}}{M_{(8,8)}}$	0.024	0.026

TABLE V: Contributions to our estimate of the exponentially-suppressed finite-volume errors.

D. Combining the finite-volume corrections

To one-loop order we write the systematic error associated with the finite-volume corrections in terms of the ratios $\Delta\mathcal{M}_{\log}/\mathcal{M}_{\text{LO}}$. These are given by:

$$\begin{aligned}
\frac{\Delta\mathcal{M}_{\log}^{27}}{\mathcal{M}_{\text{LO}}^{27}} &= \frac{1}{f^2(m_K^2 - m_\pi^2)} \left[-\frac{1}{12}m_K^4 \left(1 - \frac{m_K^2}{m_\pi^2}\right) \Delta\beta(m_\pi^2, m_K^2, m_\eta^2) \right. \\
&\quad \left. + m_K^2 \left(\frac{5}{4}\frac{m_K^4}{m_\pi^2} - \frac{13}{4}m_K^2 + 2m_\pi^2\right) \Delta\beta(m_\pi^2, m_K^2, m_\pi^2) + \right. \\
&\quad \left. (m_K^4 - 3m_\pi^2 m_K^2 + 2m_\pi^4) \Delta\beta(m_K^2, m_\pi^2, m_\pi^2) + \left(-\frac{1}{4}\frac{m_K^4}{m_\pi^2} - \frac{1}{12}m_K^2 + \frac{1}{3}m_\pi^2\right) \Delta\ell(m_\eta^2) \right. \\
&\quad \left. + \left(\frac{-m_K^4}{m_\pi^2} - 4m_K^2 + 4m_\pi^2\right) \Delta\ell(m_K^2) + \left(\frac{5}{4}\frac{m_K^4}{m_\pi^2} - \frac{45}{4}m_K^2 + 11m_\pi^2\right) \Delta\ell(m_\pi^2) \right] \quad (54)
\end{aligned}$$

and

$$\begin{aligned}
\frac{\Delta\mathcal{M}_{\log}^{88}}{\mathcal{M}_{\text{LO}}^{88}} &= \frac{1}{f^2} \left[\left(\frac{5}{4}\frac{m_K^4}{m_\pi^2} - 2m_K^2\right) \Delta\beta(m_\pi^2, m_K^2, m_\pi^2) + (m_K^2 - 2m_\pi^2) \Delta\beta(m_K^2, m_\pi^2, m_\pi^2) \right. \\
&\quad \left. + \frac{1}{4}\frac{m_K^4}{m_\pi^2} \Delta\beta(m_\pi^2, m_K^2, m_\eta^2) - \left(4 + \frac{1}{2}\frac{m_K^2}{m_\pi^2}\right) \Delta\ell(m_K^2) \right. \\
&\quad \left. + \left(\frac{5}{4}\frac{m_K^2}{m_\pi^2} - 8\right) \Delta\ell(m_\pi^2) - \frac{3}{4}\frac{m_K^2}{m_\pi^2} \Delta\ell(m_\eta^2) \right]. \quad (55)
\end{aligned}$$

The numerical values of these ratios for the 48³ and 64³ ensembles are shown in Tab. V.

VI. THE ERROR BUDGET

In this section we discuss the two remaining systematic errors: those which arise because the meson masses and the two-pion energy are not quite physical and those introduced by the perturbative Wilson coefficients. Finally all of the systematic errors in our results for the real and imaginary parts of A_2 are summarized Tables IX and X, respectively.

The volume, boundary conditions and quark masses have been chosen to enable simulations of physical $K \rightarrow \pi\pi$ decays. Nevertheless, since the volume and quark masses have to be chosen *a priori*, the output values of the meson masses and two-pion energies will be a little different from the physical values (see Tab. I). In order to estimate the corresponding uncertainty we follow the procedure described in [2, 27] and outlined below. We use measurements on 60 quenched configurations on a 24³ lattice with $a^{-1} = 1.31$ GeV performed with 3 values of the light-quark masses, 5 strange-quark masses and the application of antiperiodic boundary conditions in $n_{\text{tw}} = 0, 1, 2$ and 3 directions. These

n_{tw}	0	1	2	3
A_0	17.53(16)	17.14(73)	14.9(2.3)	24.5(9.5)
A_1	0.0273(12)	0.1038(60)	0.202(18)	0.196(82)
B_0	2.124	2.124	2.124	2.124
B_1	0.00692	0.00692	0.00692	0.00692
$\text{Re}C_0(\text{GeV})$	$1.016(55) \times 10^{-7}$	$1.43(11) \times 10^{-7}$	$1.53(25) \times 10^{-7}$	$1.78(54) \times 10^{-7}$
$\text{Re}C_1(\text{GeV})$	$1.697(89) \times 10^{-6}$	$1.29(18) \times 10^{-6}$	$1.45(38) \times 10^{-6}$	$4.22(97) \times 10^{-6}$
$\text{Re}C_2(\text{GeV})$	$2.53(51) \times 10^{-9}$	$1.08(12) \times 10^{-8}$	$1.68(25) \times 10^{-8}$	$-2(67) \times 10^{-10}$
$\text{Im}C_0(\text{GeV})$	$-1.06(31) \times 10^{-12}$	$-4.6(3.3) \times 10^{-13}$	$4.4(7.4) \times 10^{-13}$	$2(11) \times 10^{-13}$
$\text{Im}C_1(\text{GeV})$	$5.54(79) \times 10^{-11}$	$3.39(91) \times 10^{-11}$	$2.1(1.6) \times 10^{-11}$	$-1.8(3.2) \times 10^{-11}$
$\text{Im}C_2(\text{GeV})$	$-1.689(64) \times 10^{-12}$	$-1.392(66) \times 10^{-12}$	$-1.24(12) \times 10^{-12}$	$-7.5(1.9) \times 10^{-13}$

TABLE VI: Parameters used for extrapolations on the 24^3 quenched ensembles.

	(27,1)	(8,8)	(8,8) _{mx}
z_i^{LO}	0.26696	4.260055×10^{-5}	-1.0063×10^{-5}
y_i^{LO}	-0.0035185	-2.026445×10^{-4}	2.447741×10^{-4}
z_i^{NLO}	0.290342	4.70099×10^{-5}	-5.22390×10^{-5}
y_i^{NLO}	-0.00397252	-8.09555×10^{-5}	3.26016×10^{-4}

TABLE VII: Wilson coefficients at 3 GeV in the $\overline{\text{MS}}$ scheme at leading order (LO) and next-to-leading order (NLO).

measurements are used to determine the coefficients in the following phenomenological formulae:

$$m_{xy}^2 = B_0(m_x + m_y) + B_1, \quad (56)$$

$$E_{\pi\pi}^2(n_{\text{tw}}) = A_0(n_{\text{tw}})m_l + A_1(n_{\text{tw}}), \quad (57)$$

$$A_2 = C_0(n_{\text{tw}})m_s + C_1(n_{\text{tw}})m_l + C_2(n_{\text{tw}}), \quad (58)$$

where m_l and m_s are the masses of the light and strange quarks, m_{xy} is the mass of the meson consisting of x and y valence quarks (which can be either light or strange) and n_{tw} is the number of directions in which the antiperiodic boundary conditions would have to be imposed on the quenched lattice to get the correct two-pion energy. Note that n_{tw} does not have to be an integer, and is given instead by $p^2 = n_{\text{tw}}\pi^2/L^2$, where p is the centre-of-mass momentum of each pion. The full list of coefficients A, B and C obtained from these quenched configurations was presented in [27] and is reproduced in Tab. VI.

We can use the coefficients in Tab. VI to determine A_2 on the quenched ensembles for any choice of $\{m_\pi, m_K, E_{\pi\pi}\}$. We exploit this possibility for three sets of parameters: (i) the physical masses $m_K = E_{\pi\pi} = 493.7 \text{ MeV}$, $m_\pi = 139.6 \text{ MeV}$; (ii) the values from the 48^3 simulation given in the third row of Tab. I and (iii) the values from the 64^3 simulation given in the fourth row of Tab. I. We denote the corresponding three estimates of A_2 by $A_2^{\text{q:phys}}$, $A_2^{\text{q:48}}$ and $A_2^{\text{q:64}}$ respectively, where the superscript q reminds us that the results were obtained on the quenched ensembles. We use the differences $A_2^{\text{q:48}} - A_2^{\text{q:phys}}$ and $A_2^{\text{q:64}} - A_2^{\text{q:phys}}$ as estimates of the systematic error due to unphysical kinematics.

The results are:

$$\text{Re}(A_2^{\text{q:phys}}) = 2.25 \times 10^{-8} \text{ GeV}, \quad \text{Im}(A_2^{\text{q:phys}}) = -1.344 \times 10^{-12} \text{ GeV}, \quad (59)$$

$$\text{Re}(A_2^{\text{q:48}}) = 2.29 \times 10^{-8} \text{ GeV}, \quad \text{Im}(A_2^{\text{q:48}}) = -1.341 \times 10^{-12} \text{ GeV}, \quad (60)$$

$$\text{Re}(A_2^{\text{q:64}}) = 2.36 \times 10^{-8} \text{ GeV}, \quad \text{Im}(A_2^{\text{q:64}}) = -1.329 \times 10^{-12} \text{ GeV}. \quad (61)$$

The differences in Eqs. (59) - (61) translate to an estimated 1.8% error on $\text{Re}(A_2)$ and 0.2% error on $\text{Im}(A_2)$ on the 48^3 ensemble and a 4.5% difference for $\text{Re}(A_2)$ and 1.1% difference for $\text{Im}(A_2)$ on the 64^3 ensemble. These numbers are obtained from the difference of the simulated results from those at the physical point (normalized by the result at the physical point). These uncertainties are included in Tabs. IX and X under the label ‘‘unphysical kinematics’’.

To estimate the error in the Wilson coefficients, we compare the results for A_2 using Wilson coefficients calculated at leading order and next to leading order. We have used the set of coefficients evaluated in the $\overline{\text{MS}}$ scheme at 3 GeV,

	LO	NLO
$\text{Re}(A_2) 48^3$	$1.293(11) \times 10^{-8}$	$1.386(12) \times 10^{-8}$
$\text{Im}(A_2) 48^3$	$-5.551(45) \times 10^{-13}$	$-6.174(49) \times 10^{-13}$
$\text{Re}(A_2) 64^3$	$1.3410(89) \times 10^{-8}$	$1.4386(95) \times 10^{-8}$
$\text{Im}(A_2) 64^3$	$-6.037(71) \times 10^{-13}$	$-6.548(78) \times 10^{-13}$

TABLE VIII: Comparison of matrix elements calculated with leading order (LO) and next-to-leading order (NLO) Wilson coefficients.

$\text{Re}A_2$ systematic errors	48^3	64^3	cont.
NPR (nonperturbative)	0.1%	0.1%	0.1%
NPR (perturbative)	2.9%	2.5%	2.9%
Finite volume corrections	2.2%	2.4%	2.4%
Unphysical kinematics	1.8%	4.5%	4.5%
Wilson coefficients	6.8%	6.8%	6.8%
Derivative of the phase shift	1.1%	0.6%	1.1%
Total	8%	9%	9%

TABLE IX: Systematic error breakdown for $\text{Re} A_2$

which are shown in table VII [28], and the standard parametrization of Wilson coefficients was used, i.e. $C_i = z_i + \tau y_i$ where τ is the ratio of CKM matrix coefficients $\tau = -\frac{V_{ts}^* V_{td}}{V_{us}^* V_{ud}}$. The results for matrix elements calculated at leading and next-to-leading orders are shown in Tab. VIII. From the differences between the entries in the columns marked as LO and NLO we estimate that the uncertainties are 6.8% for $\text{Re}(A_2)$ on both sets of ensembles and 10% (8%) for $\text{Im}(A_2)$ on the 48^3 (64^3) ensembles.

Tables IX and X show our estimates of systematic errors associated with the results for $\text{Re}(A_2)$ and $\text{Im}(A_2)$ presented in this paper. The evaluation of the continuum limit of A_2 is discussed in following section. As will be seen, the systematic error associated with this extrapolation is negligible with respect to the statistical errors. Consequently no discretization error is shown in Tables IX and X. The values in the column marked ‘‘cont.’’ are the errors assigned to our continuum-extrapolated results, and are simply the larger of the corresponding entries from the 48^3 and 64^3 columns. We can see that the dominant contribution to the systematic error for both real and imaginary parts of A_2 on both ensembles comes from the uncertainty in Wilson coefficients.

VII. CONTINUUM EXTRAPOLATION

In this section we discuss the extrapolation of the results obtained on the 48^3 and 64^3 ensembles to the continuum limit. We divide this discussion into two parts. In the first we present the complete physical results for the complex amplitude A_2 in the continuum limit. As we will observe, the dominant error in our result comes from the perturbative error assigned to the Wilson coefficients. This may be reduced in the future if higher order perturbation theory results become available or if lattice step-scaling methods are used to allow present perturbative results to be applied at a higher energy scale. Therefore, in the second part we determine the continuum limit of the individual matrix elements themselves, normalized in the regularization-independent (\not{q}, \not{q}) and (γ, γ) schemes.

A. Continuum limit of $\text{Re}(A_2)$ and $\text{Im}(A_2)$

As already mentioned in Sec. VI the quark masses used in these ensembles are very slightly larger than their physical values. This is illustrated in Tab. XI, in which we compare the physical and simulated values of the dimensionless quantities m_π/m_Ω and m_K/m_Ω , which are highly sensitive to the light and heavy quark masses respectively. In order to determine the values of the lattice spacing we must therefore perform a short chiral extrapolation; this is achieved using a simultaneous chiral and continuum ‘global fit’ that incorporates data from both ensembles. Since the (renormalized) quark masses on the two ensembles are very similar, we must include additional ensembles in order to have a sufficient spread of masses for the determination of the chiral dependence. The full set of ensembles and

Im A_2 systematic errors	48 ³	64 ³	cont
NPR (nonperturbative)	0.1%	0.1%	0.1%
NPR (perturbative)	7.0%	6.2%	7.0%
Finite volume corrections	2.4%	2.6%	2.6%
Unphysical kinematics	0.2%	1.1%	1.1%
Wilson coefficients	10%	8%	10%
Derivative of the phase shift	1.1%	0.6%	1.1%
Total	12%	10%	12%

TABLE X: Systematic error breakdown for Im A_2

	48I	64I	phys.
m_π/m_Ω	0.08296(17)	0.08220(19)	0.08073
m_K/m_Ω	0.29740(32)	0.29982(37)	0.29643

TABLE XI: The ratios of the pion and kaon mass to the Omega baryon mass on the 48³ and 64³ ensembles as well as the physical value.

details of this procedure can be found in [7].

The determination of A_2 presented here was performed using 76 configurations of the 48³ ensemble, whereas the lattice spacings in [7] were computed using 80. In order to preserve the full correlations between the jackknife samples of A_2 and the corresponding superjackknife samples of the lattice spacing, we repeated the global fit analysis using the same 76 configurations. The details of the binning are also different. In [7] we binned the 48³ data over 5 successive measurements (100 MD time units) in order to take into account the observed autocorrelations in the data, whereas in the present calculation, as explained in Sec. II, we construct 19 bins each of 4 configurations. These differences lead to determined values of the lattice spacings in Eq. (62) below which are a little different from those in [7]. For the 64³ ensembles we use the same set of 40 configurations for the evaluation of A_2 and the same binning as in the global fit in [7].

In order to estimate the systematic errors due to the chiral extrapolation and finite volume in the determination of the lattice spacings, we have performed our fits using three different chiral ansätze: NLO SU(2) chiral perturbation theory, with and without finite-volume corrections (referred to as the ChPTFV and ChPT forms respectively), and a linear ansatz (referred to as the ‘analytic’ form). In practice we found the lattice spacings obtained from all three ansätze to be consistent to within a fraction of the statistical error due to the dominance of the near-physical data, hence we treat these systematic errors as negligible. The final results for the values of the lattice spacing are:

$$a_{64}^{-1} = 2.3584(70) \text{ GeV} \quad \text{and} \quad a_{48}^{-1} = 1.7280(41) \text{ GeV}, \quad (62)$$

where the errors are statistical only.

The lattice matrix elements M_i scale as a^3 and so small differences in the lattice spacing become amplified. We have performed the continuum extrapolation of A_2 using the lattice spacings obtained with each of the three chiral ansätze; the extrapolated values are given in Tab. XII. In figure 9 we show the continuum extrapolation in the (q, q) scheme using the lattice spacings obtained with the ChPTFV chiral ansatz. We use results obtained with this ansatz as our central values for each lattice spacing and for the extrapolated value in the continuum.

We obtain an estimate of the component of the chiral extrapolation error arising from the lattice spacing determination by taking the difference between the continuum values obtained using the ChPTFV and analytic lattice spacings. The full jackknife differences are $0.3(2.6) \times 10^{-10}$ and $0.1(1.2) \times 10^{-14}$ for the real and imaginary parts respectively. As with the lattice spacings, we cannot resolve these differences within the statistical error, hence we set the chiral error to zero. On the other hand the jackknife differences between the ChPTFV and ChPT ansätze are resolvable as they differ only in small Bessel function corrections and are thus highly correlated: we obtain $3.4(1.0) \times 10^{-11}$ and $1.59(47) \times 10^{-15}$ for the real and imaginary parts respectively. Nevertheless, these errors are only 5–8% of the statistical error and can therefore also be neglected. This leads to the result:

$$\text{Re}(A_2) = 1.501(39) \times 10^{-8} \text{ GeV} \quad \text{and} \quad \text{Im}(A_2) = -6.99(20) \times 10^{-13} \text{ GeV}, \quad (63)$$

where the errors are statistical.

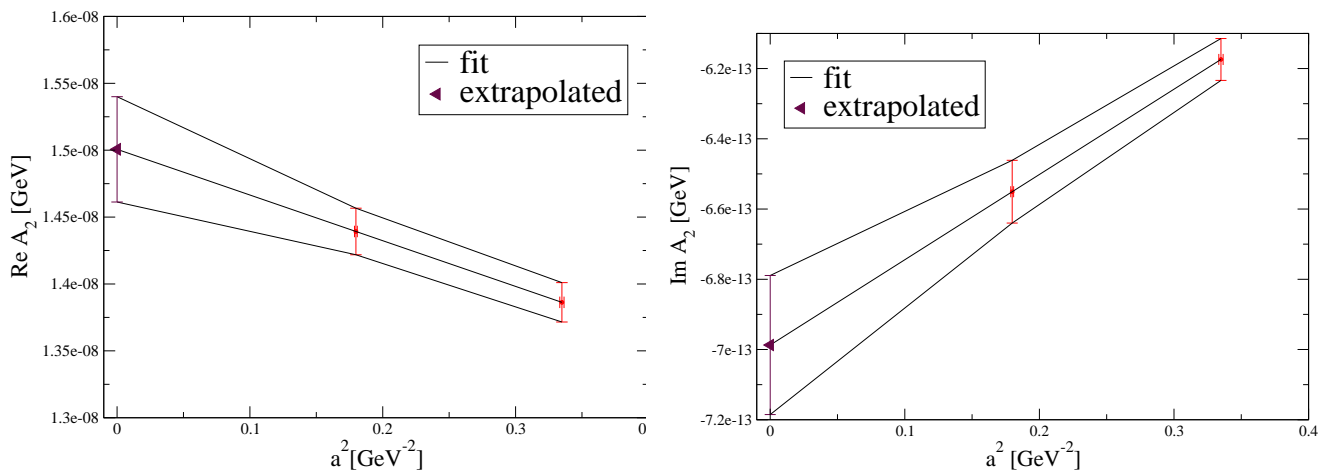


FIG. 9: The continuum extrapolation of $\text{Re}(A_2)$ (left) and $\text{Im}(A_2)$ (right). The points at finite lattice spacing are taken from Tab. III for the (\not{q}, \not{q}) intermediate renormalization scheme.

Ansatz	$\text{Re}(A_2) (\times 10^{-8} \text{ GeV})$	$\text{Im}(A_2) (\times 10^{-13} \text{ GeV})$
ChPTFV	1.501(39)	-6.99(20)
ChPT	1.494(38)	-6.96(19)
analytic	1.494(43)	-6.96(21)

TABLE XII: The continuum values of $\text{Re}(A_2)$ and $\text{Im}(A_2)$ determined using the lattice spacings obtained with each of the three chiral ansätze.

Our final result for A_2 is obtained by assigning the 9% and 12% systematic errors from Tabs. IX and X as the systematic errors to be associated with the values for $\text{Re}(A_2)$ and $\text{Im}(A_2)$ given in Eq. (63):

$$\boxed{\text{Re}(A_2) = 1.50(4)_{\text{stat}}(14)_{\text{syst}} \times 10^{-8} \text{ GeV}; \quad \text{Im}(A_2) = -6.99(20)_{\text{stat}}(84)_{\text{syst}} \times 10^{-13} \text{ GeV}.} \quad (64)$$

In order to estimate the unknown quantity $\text{Im}A_0$, we combine our results for A_2 with the experimental values of $\text{Re}A_0 = 3.3201(18) \times 10^{-7} \text{ GeV}$ and $\epsilon'/\epsilon = (1.65 \pm 0.26) \times 10^{-3}$ [29]. To this end we start by evaluating the ratio $\text{Im}A_2/\text{Re}A_2$, taking account any statistical correlations between the real and imaginary parts by performing the analysis within the jackknife procedure. On the two ensembles we find

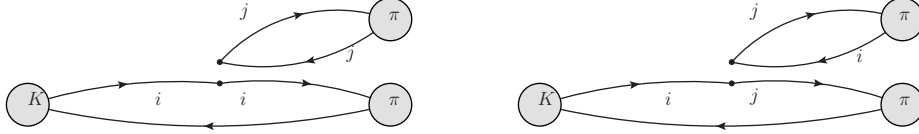
$$\left(\frac{\text{Im}A_2}{\text{Re}A_2}\right)_{483} = -4.45(5)_{\text{stat}}(65)_{\text{syst}} \times 10^{-5} \quad \text{and} \quad \left(\frac{\text{Im}A_2}{\text{Re}A_2}\right)_{643} = -4.55(5)_{\text{stat}}(62)_{\text{syst}} \times 10^{-5}. \quad (65)$$

The systematic errors for this ratio are given in Table XIII; they are generally combined in quadrature except for that due to the derivative of the phase shift because the Lellouch-Lüscher factor cancels in the ratio. It is interesting to note that if instead of adding the errors in the Wilson Coefficients for $\text{Re}A_2$ and $\text{Im}A_2$ in quadrature as in Tab. XIII, we had calculated the ratios with the coefficients at leading and next-to-leading order respectively and taken the difference as a measure of the uncertainty we would have obtained a much smaller answer (3.6% instead of 12%). Since the operators which give the dominant contributions to the real and imaginary parts are different, and in the absence of an understanding which might suggest a correlation between their Wilson coefficients, we prefer to be cautious and take the larger uncertainty. We find a similar feature in the NPR perturbative error.

The continuum extrapolation of the dimensionless ratio $\text{Re}A_2/\text{Im}A_2$ is milder than that of $\text{Re}A_2$ and $\text{Im}A_2$ separately and we obtain

$$\left(\frac{\text{Im}A_2}{\text{Re}A_2}\right)_{\text{continuum}} = -4.67(72) \times 10^{-5}. \quad (66)$$

Systematic errors in $\text{Im}A_2/\text{Re}A_2$	48^3	64^3	cont
NPR (nonperturbative)	0.1%	0.1%	0.1%
NPR (perturbative)	7.6 %	6.7 %	7.6 %
Finite volume corrections	3.5 %	3.5 %	3.5 %
Unphysical kinematics	1.8 %	4.6%	4.6%
Wilson coefficients	12.0 %	10.5 %	12.0%
Derivative of the phase shift	0	0	0
Total	14.7%	13.7%	15.3%

TABLE XIII: Systematic error breakdown for $\text{Im}A_2/\text{Re}A_2$.FIG. 10: Dominant contractions contributing to $\text{Re}(A_2) - C_1$ (left) and C_2 (right)

Using this ratio, we can calculate the electroweak penguin contribution to ϵ'/ϵ , given by:

$$\left(\frac{\epsilon'}{\epsilon}\right)_{\text{EWP}} \equiv \frac{\omega}{\sqrt{2}|\epsilon|} \frac{\text{Im}A_2}{\text{Re}A_2} = -6.6(10) \times 10^{-4}, \quad (67)$$

where we have used the values $\omega \equiv \frac{\text{Re}A_2}{\text{Re}A_0} = 0.04454(12)$ and $|\epsilon| = 2.228(11) \times 10^{-3}$ from [2]. This value for $(\epsilon'/\epsilon)_{\text{EWP}}$ is consistent with our previously quoted value $-6.25(44)(119) \times 10^{-4}$ [2]. Finally, for $\text{Im}A_0$ we find

$$\text{Im}A_0 = \text{Re}A_0 \left(\frac{\text{Im}A_2}{\text{Re}A_2} - \frac{\sqrt{2}|\epsilon|}{\omega} \frac{\epsilon'}{\epsilon} \right) = -5.40(64) \times 10^{-11} \text{ GeV}. \quad (68)$$

The results in Eqs. (67) and (68) were obtained using our result for $\text{Im}A_2/\text{Re}A_2$ in Eq. (66). If instead we take $\text{Im}A_2$ from our calculation, Eq. (64), and combine it with the experimental result $\text{Re}A_2 = 1.4787(31) \times 10^{-8} \text{ GeV}$ we obtain, $\text{Im}A_2/\text{Re}A_2 = -4.73(58) \times 10^{-5}$, $(\epsilon'/\epsilon)_{\text{EWP}} = -6.69(82) \times 10^{-4}$ and $\text{Im}A_0 = -5.42(63) \times 10^{-11} \text{ GeV}$.

B. Continuum limit of the RI-SMOM matrix elements

From the error budget in Tab. XIII we see that the dominant uncertainty is due to the Wilson coefficients, which we take to be the difference between the leading and next-to-leading order contributions as defined in [30], where the calculations were based on [31–33]. In case the Wilson coefficients in the RI-SMOM schemes become known with better precision in the future, we present in Tab. XIV the $K^+ \rightarrow \pi^+\pi^0$ matrix elements $M_i^{K^+}$ defined in Eq. (7), with the operators Q_i in Eqs. (8)–(10) renormalized in the (\not{q}, \not{q}) and (γ, γ) renormalization schemes at a renormalization scale of 3 GeV. These matrix elements together with the new Wilson coefficients would enable an improved evaluation of A_2 , without the need to recompute the matrix elements. The systematic errors for the (27,1) operator are estimated using the entries in Tab. IX with the NPR(perturbative) and Wilson coefficient errors set to zero. This gives the errors of 2.8%, 5.1% and 5.2% for the 48^3 and 64^3 ensembles and in the continuum limit respectively. For the (8,8) operators using the entries in Tab. X, the same procedure leads to systematic errors of 2.6%, 2.9% and 3.0% for the 48^3 and 64^3 ensembles and in the continuum respectively.

For completeness we also convert these three $K^+ \rightarrow (\pi\pi)_{I=2}$ matrix elements into those in the original 10 operator

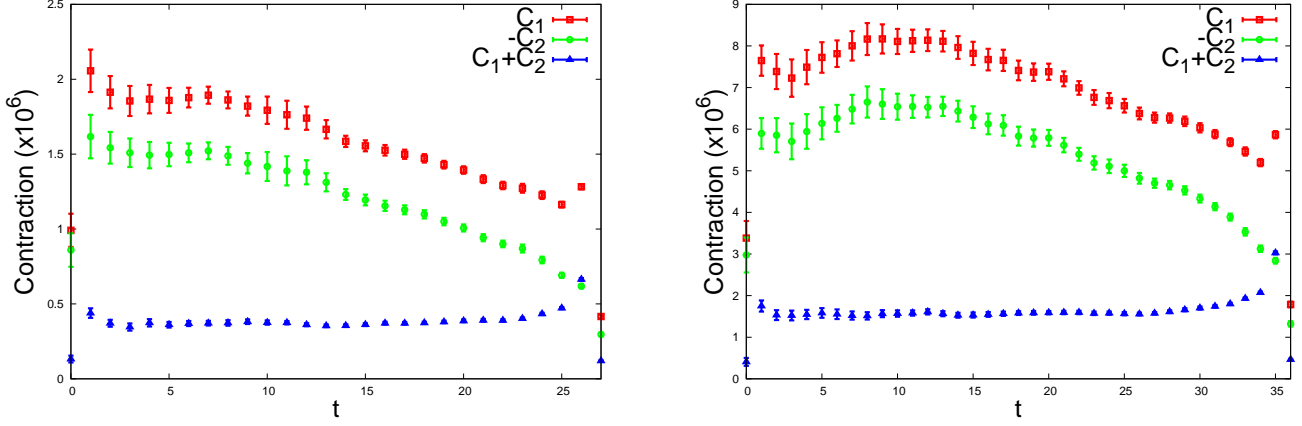


FIG. 11: Cancellation of dominant contributions to $\text{Re}(A_2)$ on the 48^3 ensembles with a $K - \pi\pi$ separation of 27 and the 64^3 ensembles with separation 36.

Ensemble	Scheme	$M_{(27,1)}^{K^+}$ [GeV^3]	$M_{(8,8)}^{K^+}$ [GeV^3]	$M_{(8,8)\text{mx}}^{K^+}$ [GeV^3]
48^3	(\not{q}, \not{q})	0.04761(39)(133)	0.7026(52)(183)	3.892(28)(101)
64^3	(\not{q}, \not{q})	0.04848(32)(247)	0.8412(88)(244)	4.140(44)(120)
48^3	(γ, γ)	0.04473(37)(128)	0.7112(53)(185)	3.471(26)(90)
64^3	(γ, γ)	0.04664(31)(238)	0.8477(88)(246)	3.724(40)(108)
Continuum	(\not{q}, \not{q})	0.0506(13)(26)	1.003(22)(30)	4.43(12)(13)
Continuum	(γ, γ)	0.0489(13)(25)	1.007(23)(30)	4.02(10)(12)

TABLE XIV: Results for the $K^+ \rightarrow (\pi\pi)_{I=2}$ matrix elements $M_i^{K^+}$ (defined in Eq. (7)) in two non-exceptional RI-SMOM renormalization schemes at the scale 3 GeV. The first error is statistical, while the second one is the systematic uncertainty estimated as described in the text.

basis as defined in [34]:

$$M_{(27,1)}^{K^+} = 3M_1^{K^+} = 3M_2^{K^+} = 2M_9^{K^+} = 2M_{10}^{K^+} \quad (69)$$

$$M_{(8,8)}^{K^+} = 2M_7^{K^+} \quad \text{and} \quad M_{(8,8)\text{mx}}^{K^+} = 2M_8^{K^+} \quad (70)$$

where $M_i^{K^+} \equiv \langle (\pi\pi)_{I=2} | Q_i | K^+ \rangle$.

VIII. CONCLUSIONS

Before briefly summarising our results and discussing prospects for future calculations we confirm our finding, first presented in [3], that there is a significant cancellation between the two dominant contributions to $\text{Re} A_2$. As explained above, $\text{Re}(A_2)$ is dominated by the matrix element of the $(27, 1)$ operator and is proportional to the sum of the two contractions C_1 and C_2 in Fig. 10. Whilst naïve factorization, frequently used for phenomenological estimates, suggests that $C_1 = 3C_2$ because of the color suppression in C_2 , we find a strong cancellation between these two contributions. For the 48^3 and 64^3 ensembles studied in this paper, we illustrate this cancellation in Fig. 11. (In Sec. III we explain that the numerical results in this paper were obtained from correlation functions with even values of $t_{\pi\pi}$. The choice of $t_{\pi\pi} = 27$ for the 48 ensembles in Fig. 11 is made to ensure that the cancellation is illustrated at the same value of $t_{\pi\pi}$ in physical units on the two sets of ensembles.) As explained in [3] we believe that this cancellation is a significant component in explaining the $\Delta I = 1/2$ rule. Although we haven't completed the calculation of A_0 at this stage, we note that the contributions of the $(27, 1)$ operator all contribute with the same sign. A similar partial cancellation occurs between the two corresponding contractions in the evaluation of the B_K parameter of neutral kaon mixing as pointed out in [35] and subsequently confirmed in [3, 36].

Our *ab initio* determination of A_2 shows clearly that phenomenological approaches based on the dominance of naïve factorization are not consistent. We note however, that there were non-lattice studies based on chiral perturbation theory and the $1/N$ expansion, where N is the number of colors, which indicated that C_2 may have the opposite sign to C_1 [37, 38]. Of course, as illustrated in our results above, the $1/N$ expansion per se is not a good approximation; C_2 is suppressed by $1/N$ and yet is comparable to C_1 . In different ways, the authors of [37, 38] combine the expansion with leading short and long-distance logarithms. In [37] the authors use an ansatz for matching the perturbative short-distance contributions and long-distance effects based on a chiral Lagrangian for mesons. In [38] the authors compare the experimental value of $\text{Re}A_2$ with the leading term of the expansion to deduce that C_2 should be negative. For recent discussions of these two early approaches, stimulated by our lattice QCD result [1, 2] and written by subsets of their original authors, we refer the reader to [39, 40].

Our earlier calculation of A_2 was performed on an ensemble at a single coarse lattice spacing, $a^{-1} = 1.364 \text{ GeV}$ [1, 2], and so not surprisingly the dominant systematic uncertainty was due to discretization errors. We estimated these to be about 15%, although with only a single lattice spacing this could only be an estimate. In the present paper we repeat and refine the earlier calculation which is now performed on two finer ensembles with different lattice spacings, allowing for a continuum extrapolation. We have determined $\text{Re}A_2$ to be $1.50(4)_{\text{stat}}(14)_{\text{sys}} \times 10^{-8} \text{ GeV}$. This is consistent with the experimental values of $1.4787(31) \times 10^{-8} \text{ GeV}$ from charged kaon decays and $1.570(53) \times 10^{-8} \text{ GeV}$ from neutral kaon decays. We have also calculated the imaginary part of A_2 to be $-6.93(20)_{\text{stat}}(84)_{\text{sys}} \times 10^{-13} \text{ GeV}$, which was unknown until [1, 2]. (We recall that the corresponding results from our earlier work were $\text{Re}A_2 = 1.38(5)_{\text{stat}}(26)_{\text{sys}} \times 10^{-8} \text{ GeV}$ and $\text{Im}A_2 = -6.54(46)_{\text{stat}}(120)_{\text{sys}} \times 10^{-8} \text{ GeV}$.) Our results for Im and $\text{Re}A_2$ imply, $(\epsilon'/\epsilon)_{EWP} = -6.6(10) \times 10^{-4}$. This can be compared to the result obtained via Finite Energy Sum Rules [41], $\text{Re}(\epsilon'/\epsilon)_{EWP} = -(11.0 \pm 3.6) \times 10^{-4}$ (see also results based on vacuum saturation [41, 42]).

The errors are currently dominated by systematic uncertainties, the largest of which is due to the uncertainty in the (perturbative) evaluation of the Wilson coefficients (see Tabs. IX and X). It is testimony to the huge progress in the precision of lattice calculations that this is the case. We have aimed to be conservative in estimating this error, taking the difference between the lowest order and the next-to-lowest order as the uncertainty. The natural way to decrease this error is to perform higher-order perturbative calculations in the standard model but it may also be possible to use step scaling to increase the renormalization scale in the intermediate schemes (such as the RI-SMOM schemes used in this study) and hence to increase the scale at which the matching to the $\overline{\text{MS}}$ scheme is performed and at which the Wilson coefficients are calculated. It will be interesting to explore this possibility.

In order to have a fully quantitative understanding of the $\Delta I = 1/2$ rule and to determine ϵ'/ϵ and to compare the result to the experimental value $\epsilon'/\epsilon = (1.65 \pm 0.26) \times 10^{-3}$ we need to perform the evaluation of A_0 at physical kinematics. A key ingredient which makes the calculation of A_2 feasible is the use of the Wigner-Eckart theorem described in Sec. III. Together with the choice of volume and the use of antiperiodic boundary conditions for the d -quark in all 3 spatial directions, it ensures that the energy of the two-pion ground state is equal to m_K . Unfortunately this approach cannot be directly applied to the calculation of A_0 , in particular the breaking of isospin symmetry by the boundary conditions invalidates the calculation. For example, the π^0 remains at rest with the antiperiodic boundary conditions, whereas the charged pions have non-zero momentum. More sophisticated boundary conditions mixing quarks and anti-quarks and an isospin rotation, the so called *G-parity* boundary conditions [11, 43–46], must therefore be used instead for both the valence and the sea quarks. The evaluation of A_0 with G-parity boundary conditions is well underway and exciting progress has recently been reported in [4] and we anticipate the first complete calculation of A_0 , albeit on a single lattice spacing, within the next year.

Acknowledgements

The generation of the $48^3 \times 96$ and $64^3 \times 128$ Möbius DWF+Iwasaki ensembles used to calculate A_2 was performed using the IBM Blue Gene/Q (BG/Q) Mira machine at the Argonne Leadership Class Facility (ALCF) provided under the Incite Program of the US DOE, on the STFC funded DiRAC BG/Q system in the Advanced Computing Facility at the University of Edinburgh, and on the BG/Q machines at Brookhaven National Laboratory (BNL). The DiRAC equipment was funded by BIS National E-infrastructure capital grants ST/K000411/1, STFC capital grant ST/H008845/1, and STFC DiRAC Operations grants ST/K005804/1 and ST/K005790/1. DiRAC is part of the National E-Infrastructure. Most of the measurements were also performed on the DiRAC and Mira machines, with the remainder performed using the Brookhaven and the RIKEN-BNL Research Center BG/Q computers at BNL. The software used includes the CPS QCD code (<http://qcdoc.phys.columbia.edu/cps.html>), supported in part by the USDOE SciDAC program; the BAGEL (<http://www2.ph.ed.ac.uk/~paboyle/bagel/Bagel.html>) assembler kernel generator for high-performance optimized kernels and fermion solvers [47]. The gauge fixing for the 48I ensemble was performed using the CUTH cluster at Columbia University using the "GLU" (Gauge Link Utility) codebase (<https://github.com/RJhudspith/GLU>).

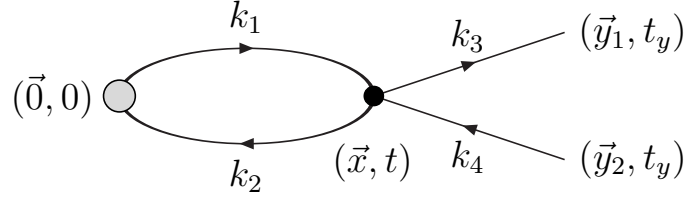


FIG. 12: Contribution to the correlation function in which two pions are produced by an operator at the origin (grey circle), and rescatter by the strong interactions denoted by the filled circle.

T.B. is supported in part by the US Department of Energy Grant No. DE-FG02-92ER41989, N.H.C., R.D.M., D.Z. and H.Y. by US DOE Grant No. DE-SC0011941, N.G. by Leverhulme Research grant RPG-2014-118 and by the European Union under Grant Agreement number 238353 (ITN STRONGnet), C.J. and A. S. by U.S. DOE contract DE-AC02-98CH10886(BNL) and T.J. and C.T.S. by UK STFC Grants ST/G000557/1 and ST/L000296/1. C.K. is supported by a RIKEN foreign postdoctoral research (FPR) grant.

Appendix A: $\beta(m_K, m_\pi, m_\pi)$ and the Lellouch-Lüscher Factor

In Sec. V we use chiral perturbation theory to estimate the finite-volume corrections in our calculation of A_2 and consider the differences between the finite-volume sums and infinite-volume integrals in $\ell(m^2)$ and $\beta(q, m_1, m_2)$ defined in Eqs. (47) and (48). In the case with $q = (m_K, \vec{0})$ and $m_1 = m_2 = m_\pi$, $\beta(m_K, m_\pi, m_\pi)$ in Minkowski space has an imaginary part which leads to finite-volume corrections in Euclidean space which decrease only as inverse powers of the volume and not exponentially. These power corrections are the one-loop chiral perturbation theory (NLO ChPT) contributions to the Lellouch-Lüscher factor F in Eqs. (40) and (41). This factor is included fully in our analysis and so we must not include it again from NLO ChPT. A detailed study of how the Lellouch-Lüscher factor arises in one-loop ChPT was performed in [5], but we hope that it will be useful to summarise the main points here.

In Minkowski space, performing the k_0 integration in the centre-of-mass frame we obtain

$$\beta(m_K, m_\pi, m_\pi) = \int \frac{d^3 \vec{k}}{(2\pi)^3} \frac{1}{\omega(\vec{k}) [m_K^2 - 4\omega^2(\vec{k}) + i\epsilon]}, \quad (\text{A1})$$

where $\omega^2(\vec{k}) = |\vec{k}|^2 + m_\pi^2$.

In finite-volume Euclidean space we evaluate the correlation function illustrated in Fig. 12. The kaon propagator is irrelevant for our discussion and so we amputate it, and consider the two pions to be created at the origin, to rescatter and to be annihilated on the timeslice at t_y . After performing the integrals over \vec{y}_1, \vec{y}_2 (with phase factors $e^{i\vec{q}\cdot\vec{y}_1}$ and $e^{-i\vec{q}\cdot\vec{y}_2}$ respectively) and \vec{x} and exploiting the resulting δ functions, we obtain for this contribution to the correlation function:

$$I \equiv \int_{-\infty}^{\infty} dt \int \frac{d^3 \vec{k}}{(2\pi)^3} \prod_{i=1}^4 \frac{dE_i}{E_i^2 + \omega_i^2} e^{i(E_1 - E_2)t} e^{i(E_3 - E_4)(t_y - t)}, \quad (\text{A2})$$

where in a finite volume the integral over \vec{k} is replaced by the corresponding sum. Here $\omega_1^2 = \omega_2^2 = \omega^2(\vec{k}) = |\vec{k}|^2 + m_\pi^2$ and $\omega_3^2 = \omega_4^2 = \omega^2(\vec{q}) = |\vec{q}|^2 + m_\pi^2$ so that $\omega_{3,4}$ are not integration variables.

The energy integrals can now be performed by contour integration; there are 3 contributions depending on the value of t .

1. The first contribution is from the interval $-\infty < t < 0$ and gives

$$I_1 = \frac{e^{-2\omega(\vec{q})t_y}}{32\omega^2(\vec{q})} \int \frac{d^3 \vec{k}}{(2\pi)^3} \frac{1}{\omega^2(\vec{k}) (\omega(\vec{k}) + \omega(\vec{q}))}. \quad (\text{A3})$$

2. The second contribution comes from the region $0 < t < t_y$ and gives

$$I_2 = \frac{e^{-2\omega(\vec{q})t_y}}{32\omega^2(\vec{q})} \int \frac{d^3\vec{k}}{(2\pi)^3} \frac{1}{\omega^2(\vec{k}) (\omega(\vec{k}) - \omega(\vec{q}))} (1 - e^{-2(\omega(\vec{k}) - \omega(\vec{q}))t_y}). \quad (\text{A4})$$

3. Finally we have the contribution from the region $t_y < t < \infty$ which gives

$$I_3 = \frac{1}{32\omega^2(\vec{q})} \int \frac{d^3\vec{k}}{(2\pi)^3} \frac{e^{-2\omega(\vec{k})t_y}}{\omega^2(\vec{k}) (\omega(\vec{k}) + \omega(\vec{q}))}. \quad (\text{A5})$$

The contribution to the amplitude is given by the coefficient of

$$\frac{e^{-2\omega(\vec{q})t_y}}{4\omega^2(\vec{q})}.$$

In finite volume the integrals over \vec{k} are replaced by the corresponding sums and we obtain the following three contributions.

$$T_1 = \frac{1}{8L^3} \sum_{\vec{k}} \frac{1}{\omega^2(\vec{k}) (\omega(\vec{k}) + \omega(\vec{q}))} \quad (\text{A6})$$

from the region $t < 0$.

$$T_2 = \left(\frac{\nu_q t_y}{L^3} \right) \frac{1}{4\omega^2(\vec{q})} + \frac{1}{8L^3} \sum_{|\vec{k}| \neq |\vec{q}|} \frac{1}{\omega^2(\vec{k}) (\omega(\vec{k}) - \omega(\vec{q}))}, \quad (\text{A7})$$

from the region $0 < t < t_y$, where ν_q is the degeneracy of states with $\vec{k} = \vec{q}$. The term proportional to t_y is the FV correction to the two-pion energy and it can be checked that this is correctly given by the Lüscher quantization condition [5]. Finally from the region $t_y < t < \infty$ we have

$$T_3 = \left(\frac{\nu_q}{L^3} \right) \frac{1}{16\omega^3(\vec{q})}. \quad (\text{A8})$$

We now separate the terms with $|\vec{k}| = |\vec{q}|$ from those where $|\vec{k}| \neq |\vec{q}|$. When $|\vec{k}| = |\vec{q}|$, we find a contribution

$$\frac{\nu_q}{L^3} \frac{1}{4\omega^2(\vec{q})} \left\{ \frac{1}{4\omega(\vec{q})} + \frac{1}{4\omega(\vec{q})} \right\}, \quad (\text{A9})$$

where the first term in the braces corresponds to T_1 and the second corresponds to T_3 . The contribution from T_3 is cancelled by the FV correction to the matrix element of the two-pion interpolating operator at t_y [5] whereas the one from T_1 is a contribution to the FV effects in the amplitude.

The contributions from $|\vec{k}| \neq |\vec{q}|$ come from T_1 and T_2 and can be combined to give

$$\frac{1}{4L^3} \sum_{|\vec{k}| \neq |\vec{q}|} \frac{1}{\omega(\vec{k}) (\omega^2(\vec{k}) - \omega^2(\vec{q}))}. \quad (\text{A10})$$

Thus in Euclidean finite volume we obtain

$$S'_1 + \frac{\nu_q}{16L^3 E^3}, \quad (\text{A11})$$

where it is convenient to define

$$S'_n = \frac{\omega^{n-1}(\vec{q})}{4L^3} \sum_{|\vec{k}| \neq |\vec{q}|} \frac{1}{\omega^n(\vec{k}) (\omega^2(\vec{k}) - \omega^2(\vec{q}))} \quad (\text{A12})$$

and the corresponding integrals by

$$J_n = \frac{\omega^{n-1}(\vec{q})}{4} \mathcal{P} \int \frac{d^3 \vec{k}}{(2\pi)^3} \frac{1}{\omega^n(\vec{k}) (\omega^2(\vec{k}) - \omega^2(\vec{q}))}. \quad (\text{A13})$$

Relating this sum to the corresponding integral gives the LL-factor [5]. We now make this more specific and determine the exponentially small corrections. In the difference $S'_1 - S'_0$ there is no term with a pole at $\omega(k) = \omega(q)$ so that this difference can be related to the corresponding integral using the Poisson summation formula and the exponentially small finite-volume corrections can be identified

$$S'_1 - S'_0 = -\frac{1}{4L^3\omega(\vec{q})} \sum_{|\vec{k}| \neq |\vec{q}|} \frac{1}{\omega(\vec{k})(\omega(\vec{k}) + \omega(\vec{q}))} \quad (\text{A14})$$

$$\begin{aligned} &= -\frac{1}{4L^3\omega(\vec{q})} \sum_{\vec{k}} \frac{1}{\omega(\vec{k})(\omega(\vec{k}) + \omega(\vec{q}))} + \frac{\nu_q}{8L^3\omega^3(\vec{q})} \\ &= J_1 - J_0 + \frac{\nu_q}{8L^3\omega^3(\vec{q})} + e_{1,0}. \end{aligned} \quad (\text{A15})$$

Thus we see that the finite volume and infinite-volume results are related by

$$S'_1 + \frac{\nu_q}{16L^3E^3} = J_1 - J_0 + S'_0 + \frac{3\nu_q}{16L^3E^3} + e_{1,0}, \quad (\text{A16})$$

where $e_{1,0}$ represent the exponentially small corrections,

$$e_{1,0} = -\frac{1}{8\pi^2\omega(\vec{q})L} \sum_{\vec{n}, n \neq 0} \frac{1}{n} \int_0^\infty k dk \frac{\sin(nkL)}{\omega(k)(\omega(k) + \omega(q))}, \quad (\text{A17})$$

and n and k are $|\vec{n}|$ and $|\vec{k}|$ respectively. It was shown in [5] that $-J_0 + S'_0 + \frac{3\nu_q}{16L^3E^3}$ is precisely the one-loop contribution to the Lellouch-Lüscher factor. The residual exponentially small finite-volume effects are given by $e_{1,0}$. (The ultraviolet divergence cancels in the difference $J_0 - S'_0$, but if the zeta function regularization is used, as in [22], then $J_0 = 0$.)

We have presented the above detailed discussion because we believe that there is a misunderstanding in the literature. In Eqs. (71) and (73) of [6], the authors take the finite-volume corrections in $\beta(m_K, m_\pi, m_\pi)$ in Euclidean space to be the difference between the momentum integral and the corresponding sum over the integrand in Eq. (A1) but with the replacement $m_K^2 - 4\omega^2(k) \rightarrow m_K^2 + 4\omega^2(k)$ in the denominator. Since there would now be no singularity in the denominator, the finite-volume corrections would be exponential and there would be no Lellouch-Lüscher factor. The above derivation demonstrates instead the origin of the power corrections in the volume.

Throughout the above discussion we assumed periodic boundary conditions in all three spatial directions so that $k_i = n_i \times (2\pi/L)$ where n_i is an integer. In our determination of A_2 we use antiperiodic boundary conditions in all three directions so that

$$e_{1,0} = -\frac{1}{8\pi^2\omega(q)L} \sum_{\vec{n}, n \neq 0} \frac{(-1)^{n_x+n_y+n_z}}{n} \int_0^\infty k dk \frac{\sin(nkL)}{\omega(k)(\omega(k) + \omega(q))}. \quad (\text{A18})$$

-
- [1] T. Blum, P. A. Boyle, N. H. Christ, N. Garron, E. Goode, T. Izubuchi, C. Jung and C. Kelly *et al.*, Phys. Rev. Lett. **108** (2012) 141601 [arXiv:1111.1699 [hep-lat]].
 - [2] T. Blum, P. A. Boyle, N. H. Christ, N. Garron, E. Goode, T. Izubuchi, C. Jung and C. Kelly *et al.*, Phys. Rev. D **86** (2012) 074513 [arXiv:1206.5142 [hep-lat]].
 - [3] P. A. Boyle *et al.* [RBC and UKQCD Collaborations], Phys. Rev. Lett. **110** (2013) 152001 [arXiv:1212.1474 [hep-lat]].
 - [4] C. Kelly and D. Zhang, [RBC and UKQCD collaborations], PoS LATTICE **2014**, 365 and 366 (2014).
 - [5] C. J. D. Lin, G. Martinelli, E. Pallante, C. T. Sachrajda and G. Villadoro, Nucl. Phys. B **650** (2003) 301 [hep-lat/0208007].

- [6] C. Aubin, J. Laiho, S. Li and M. F. Lin, Phys. Rev. D **78** (2008) 094505 [arXiv:0808.3264 [hep-lat]].
- [7] T. Blum *et al.* [RBC and UKQCD Collaborations], arXiv:1411.7017 [hep-lat].
- [8] R. C. Brower, H. Neff and K. Orginos, arXiv:1206.5214 [hep-lat].
- [9] A. Stathopoulos and K. Orginos, SIAM J. Sci. Comput. **32** (2010) 439 [arXiv:0707.0131 [hep-lat]].
- [10] T. Blum, T. Izubuchi and E. Shintani, Phys. Rev. D **88** (2013) 094503 [arXiv:1208.4349 [hep-lat]].
- [11] C. Kim, Nucl. Phys. Proc. Suppl. **129** (2004) 197-199. [hep-lat/0311003].
- [12] C. H. Kim, Nucl. Phys. Proc. Suppl. **140** (2005) 381-383.
- [13] C. Sturm, Y. Aoki, N. H. Christ, T. Izubuchi, C. T. C. Sachrajda and A. Soni, Phys. Rev. D **80** (2009) 014501 [arXiv:0901.2599 [hep-ph]].
- [14] G. Martinelli, C. Pittori, C. T. Sachrajda, M. Testa and A. Vladikas, Nucl. Phys. B **445** (1995) 81 [hep-lat/9411010].
- [15] A. Donini, V. Gimenez, G. Martinelli, M. Talevi and A. Vladikas, Eur. Phys. J. C **10** (1999) 121 [hep-lat/9902030].
- [16] R. Arthur, P. A. Boyle, N. Garron, C. Kelly, A. T. Lytle, Phys. Rev. D **85** (2012) 014501 [arXiv:1109.1223 [hep-lat]].
- [17] Y. Aoki, T. Blum, N. H. Christ, C. Dawson, T. Izubuchi, R. D. Mawhinney, J. Noaki and S. Ohta *et al.*, Phys. Rev. D **73** (2006) 094507 [hep-lat/0508011].
- [18] N. Christ [RBC and UKQCD Collaborations], PoS LAT **2005** (2006) 345.
- [19] P. Boyle *et al.* [RBC-UKQCD Collaboration], PoS LATTICE **2010** (2010) 307 [arXiv:1101.5579 [hep-lat]].
- [20] M. Gockeler, R. Horsley, H. Oelrich, H. Perlt, D. Petters, P. E. L. Rakow, A. Schafer and G. Schierholz *et al.*, Nucl. Phys. B **544** (1999) 699 [hep-lat/9807044].
- [21] C. Lehner and C. Sturm, Phys. Rev. D **84**, 014001 (2011) [arXiv:1104.4948 [hep-ph]].
- [22] L. Lellouch and M. Lüscher, Commun. Math. Phys. **219** (2001) 31 [hep-lat/0003023].
- [23] A. Schenk, Nucl. Phys. B **363** (1991) 97.
- [24] J. Laiho and A. Soni, Phys. Rev. D **65** (2002) 114020 [hep-ph/0203106].
- [25] C. Aubin and C. Bernard, Phys. Rev. D **68** (2003) 034014 [hep-lat/0304014].
- [26] C. h. Kim, C. T. Sachrajda and S. R. Sharpe, Nucl. Phys. B **727** (2005) 218 [hep-lat/0507006].
- [27] Matthew Lighman, Columbia University Doctoral Thesis (2011).
- [28] Elaine Goode, Southampton University Doctoral Thesis (2012).
- [29] K. A. Olive *et al.* [Particle Data Group Collaboration], Chin. Phys. C **38** (2014) 090001.
- [30] G. Buchalla, A. J. Buras and M. E. Lautenbacher, Rev. Mod. Phys. **68** (1996) 1125 [hep-ph/9512380].
- [31] A. J. Buras, M. Jamin and M. E. Lautenbacher, Nucl. Phys. B **408** (1993) 209 [hep-ph/9303284].
- [32] M. Ciuchini, E. Franco, G. Martinelli and L. Reina, Phys. Lett. B **301** (1993) 263 [hep-ph/9212203].
- [33] M. Ciuchini, E. Franco, G. Martinelli, L. Reina and L. Silvestrini, Z. Phys. C **68** (1995) 239 [hep-ph/9501265].
- [34] T. Blum *et al.* [RBC Collaboration], Phys. Rev. D **68** (2003) 114506 [hep-lat/0110075].
- [35] L. Lellouch, arXiv:1104.5484 [hep-lat].
- [36] N. Carrasco *et al.* [ETM Collaboration], Phys. Lett. B **736** (2014) 174 [arXiv:1312.6691 [hep-lat]].
- [37] W. A. Bardeen, A. J. Buras and J. M. Gerard, Phys. Lett. B **192** (1987) 138.
- [38] A. Pich and E. de Rafael, Phys. Lett. B **374** (1996) 186 [hep-ph/9511465].
- [39] A. J. Buras, J. M. Gérard and W. A. Bardeen, Eur. Phys. J. C **74** (2014) 5, 2871 [arXiv:1401.1385 [hep-ph]].
- [40] A. Pich, arXiv:1410.3783 [hep-ph].
- [41] V. Cirigliano, J. F. Donoghue, E. Golowich and K. Maltman, Phys. Lett. B **555** (2003) 71 [hep-ph/0211420].
- [42] A. J. Buras and M. Jamin, JHEP **0401** (2004) 048 [hep-ph/0306217].
- [43] U. J. Wiese, Nucl. Phys. B **375** (1992) 45.
- [44] C. Kim and N. H. Christ, PoS LAT **2009**, 255 (2009) [arXiv:0912.2936 [hep-lat]].
- [45] C. Kelly [RBC and UKQCD Collaborations], PoS LATTICE **2012** (2012) 130.
- [46] C. Kelly, T. Blum, N. H. Christ, A. Lytle and C. Sachrajda, PoS LATTICE **2013** (2013) 401.
- [47] P. Boyle, Comput. Phys. Commun. **180** (2009) 2739-2748